



California State University **Chico**

EECE 653 Software Defined Radio  
Lab 2 Amplitude Modulation (AM)  
Demodulator

Yolanda D. Reyes

October 2, 2024

# Table of Contents

|  |             |
|--|-------------|
| 1. Introduction  |             |
| 1.1 Digital Communication Systems .....  | pp. 1 - 7   |
| 2. Calculations  |             |
| 2.1 Filter Design based on Calculations for Time Constants $\tau_1$ and $\tau_2$ ..... | pp. 7 - 8   |
| 2.2 Time Domain to Z-Domain Transformation .....                                       | pp. 8 - 10  |
| 2.3 Envelope Detector: Rectifier Only .....  | pp. 10 - 11 |
| 2.4 Envelope Detector: Rectifier and LPF .....   | pp. 11      |
| 2.5 Extended Envelope Detector: Rectifier Only .....                                   | pp. 12 - 13 |
| 2.6 Extended Envelope Detector: Rectifier and LPF .....                                | pp. 13 - 14 |
| 3. Simulations   |             |
| 3.1 MATLAB: Spectrum Analyzer Simulation .....   | pp. 15 - 16 |
| 3.2 LtSPICE: $V_{out}$ vs. $V_{in}$ .....  | pp. 16 - 20 |
| 4. Experimental Results  |             |
| 4.1 Envelope Detector: Rectifier Only .....  | pp. 21 - 22 |
| 4.2 Envelope Detector: Rectifier and LPF .....   | pp. 23 - 24 |
| 4.3 Extended Envelope Detector: Rectifier Only .....                                   | pp. 25 - 26 |
| 4.4 Extended Envelope Detector: Rectifier and LPF .....                                | pp. 27 - 32 |
| 5. Results and Conclusion  |             |
| 5.1 Results .....  | pp. 33      |
| 5.2 Discussion .....   | pp. 33      |
| 5.3 Conclusion .....   | pp. 34      |
| 6. Datasheets  |             |
| Diode: 1N4148 Datasheet .....  | pp. 35 - 37 |
| 7. References .....  | pp. 38- 39  |

# 1. Introduction

## 1.1. Digital Communication Systems

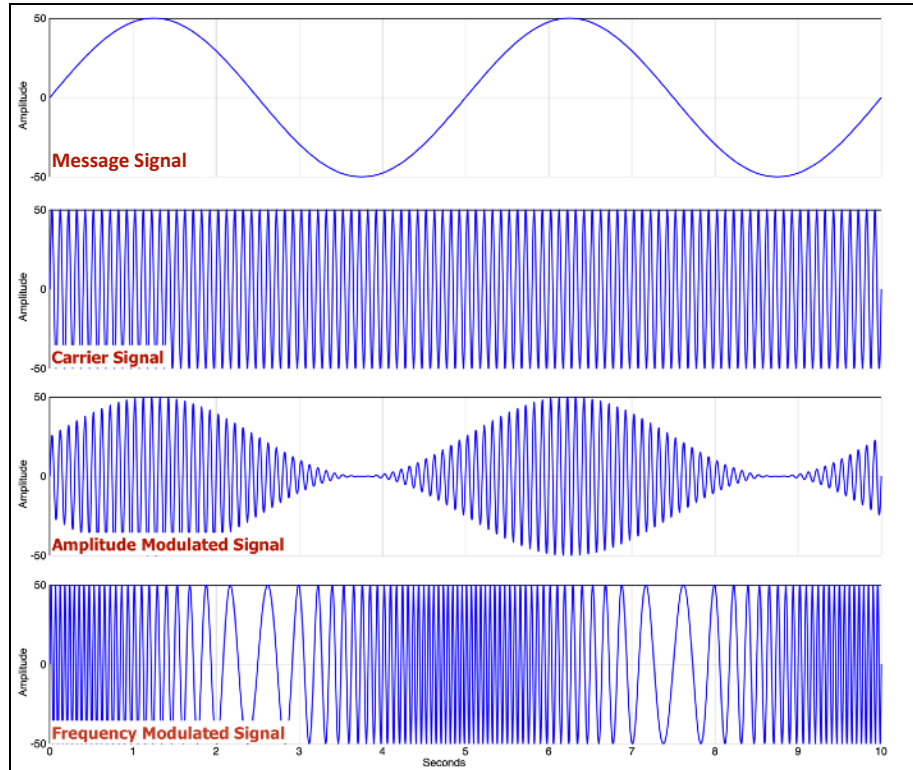
Traditional radio frequency (RF) communication systems can trace their origin back to 1886 when Heinrich Hertz built the first apparatus for generating and detecting radio waves [1]. One of the first widely utilized RF communication systems developed in the 1890s is morse code which was transmitted using radiotelegraphy [2,3]. Early RF communication systems required specific hardware to generate, modulate, transmit and receive RF signals. Because of this hardware dependency pre-software defined radio (SDR) systems were not flexible and only capable of operating under the restrictions set by the hardware. Over the past 130+ years many standards and protocols such as the International Telecommunication Union (ITU-T) standard for audio copanding, G.711, the audio codec protocol G.722, and the Internet Protocol Suite (TCP/IP) have been widely adopted and are still in use today [4,5,6]. The rapidly evolving telecommunication landscape meant that with each new protocol or standard existing systems needed their hardware redesigned to stay in compliance with newest conventions. Because of the development and improvement of electronics components such as the integrated circuit (IC), analog-to-digital converters (ADC), and digital-to-analog converters (DAC) a transition away from the hardware restricted traditional RF communication systems towards flexible software defined radio (SDR) systems could be realized [7,8,9,10].

SDR systems employ several improved techniques such as digital signal processing (DSP), direct digital synthesis (DDS), and signal modulation. Before DSP traditional RF communication systems performed filtering, modulation, demodulation and amplification via analog circuits using resistors, capacitors, inductors, and operational amplifiers tuned to specific behaviors. DSP improved these areas of RF systems by enabling the hardware to stay fixed, while providing flexibility by using software programming to implement variability of these key features. Modulation, the act of combining a carrier signal with a message signal for transmission, demodulation, the act of extracting the original message signal from the carrier signal after receiving, filtering, the enhancing and attenuating of specific frequencies of interest and amplification, when implemented in SDR systems, use Discrete Fourier Transform (DFT), Fast Fourier Transform (FFT), scalar multiplication and convolution algorithms to achieve flexibility with the fixed hardware. Generating precise and stable frequency wave forms also improved to enable SDR.

Analog signal synthesis in pre-SDR FM communication systems employed analog components such as Voltage-Controlled Oscillators (VCOs), and Phase-Locked Loops (PLLs) to achieve precise frequency waveform generation. While these components are still used in the hardware of SDR systems there is no need to create VCOs or PLLs for every possible waveform of interest. By implementing a phase accumulator, which increments by one phase step at each clock cycle, and calculating step size, the SDR system is capable of

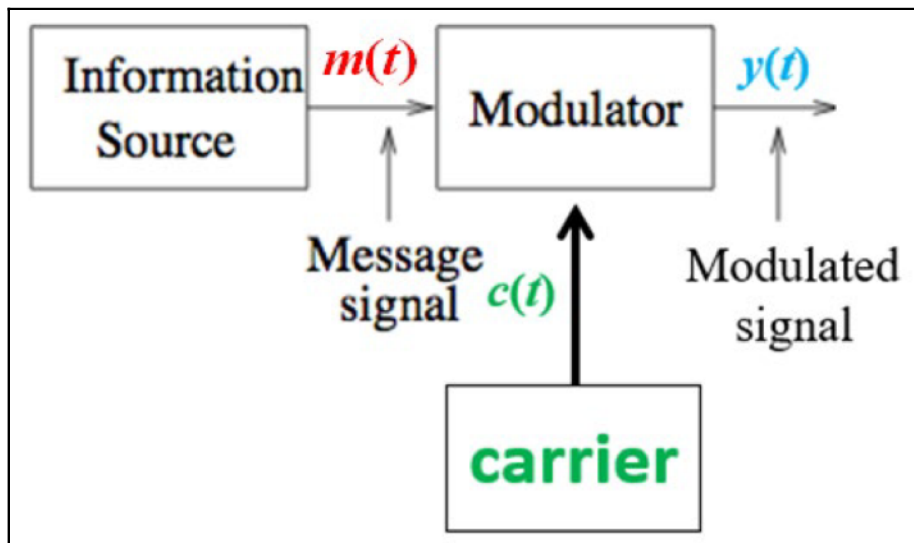
generating precise frequencies. The limiting factor in this type of waveform generation shifts from hardware based limitations to frequency resolution which is dependent on the number of bits in the phase accumulator, and the DAC which determines how finely the output waveform's amplitude can be represented. Major advantages with SDR over traditional FM communication systems includes the ability for rapid tuning, quick frequency adjustments "hopping", and lower phase noise. These advantages enable complex, multi-frequency and phase coherent waveforms to be dynamically generated which also provide an SDR system with multi-functionality and multi-mode capabilities. Being able to generate a wide range of frequency waveforms in software is a crucial task in modern communication systems. Signal modulation methods are equally important to modern communication systems and benefit greatly when implemented in an SDR paradigm.

Traditional RF communication systems require dedicated hardware designs to provide access to modulation schemes, seen in Fig. 1, such as Amplitude Modulation (AM), and Frequency Modulation (FM). However in an SDR system software provides the flexibility of switching between schemes which is essential in multi-mode communication devices such as smartphones which use protocols such as Global System for Mobile Communications (GSM), Code-Division Multiple Access (CDMA) and Long Term Evolution (LTE).



**Fig. 1** Plots of a message signal,  $m(t)$ , carrier signal,  $c(t)$ , with both the Amplitude Modulation (AM) scheme, and Frequency Modulation (FM) scheme applied resulting in output signal  $y(t)$ . These two popular modulation methods are used to transmit encoded data with a carrier signal. By analyzing the modulation effects  $m(t)$  has on  $c(t)$  data is extracted from the transmitted signal. Image © 2022 Brian Pickle [11].

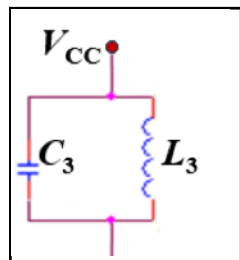
In early telecommunication systems the AM scheme was implemented using modulator tubes and a signal mixer, in modern non-SDR systems the analog components required to achieve the AM scheme include an oscillator to produce the carrier signal, a modulator to produce the data signal and an operational amplifier. The benefit of utilizing an SDR system to implement the AM scheme is in the leveraging of algorithms to digitally combine the message signal and the carrier signal in the modulator block, showcased in Fig. 2. It is important to note that with the AM scheme noise greatly affects the amplitude, which is the feature that carries the information. Because of this susceptibility to data loss due to noise, the FM scheme was developed.



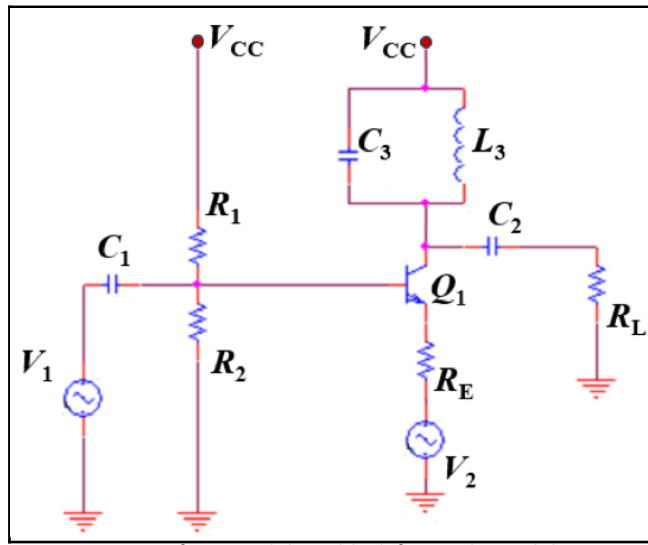
**Fig. 2** Diagram of message signal  $m(t)$ , carrier signal,  $c(t)$ , entering the modulator/signal mixer block in a RF communication system. The modulation process must be efficient to ensure the transmitted signal is strong enough with a low signal-to-noise ratio so that it can be received over long distances with data integrity maintained. Analog components in modern modulator blocks include transistors which replaced vacuum tubes capable of handling the high power required for broadcasting. Image © 2024 Dr. Ghang-Ho Lee.

In Fig. 3 a typical SDR transmitter system is presented [12]. The Data Source block is where the information originates which can be sound, video, text, etc. The Source Encoder block compresses/encodes, the data which will enable a reduction in transmission bandwidth requirements without significant loss of information. Some common compression algorithms include MPEG and H.264. The Channel Encoder is vital in error detection and correction before modulation, DAC, and ultimately transmission by improving the resiliency of data during transmission over noisy channels. Depending on the SDR system implementation the convolutional algorithm may be deployed in the Channel Encoder to support data integrity regardless of errors during transmission because it is easy to implement in software. The Symbol Modulator utilizes software techniques that map bits to symbols which indicate changes in amplitude, frequency or phase depending on the transmission modulation scheme selected.

Lab 1 work is focused on the Symbol Modulator block, in Fig. 2 & 3. For Lab 1 it is assumed that the message signal,  $m(t)$ , has already been processed by the Source and Channel Encoders presented in Fig. 3. A key concept explored in Lab 1 is the tuning of the modulator block by varying capacitor  $C_3$  in the tank circuit presented in Fig. 4. In Fig. 5 the tank circuit is connected to  $V_{cc}$  and the collector port of NPN BJT  $Q_1$  this implementation determines how much voltage and power is delivered to  $R_L$ . Considering the next circuit modules in the AM transmitter would be the DAC, and an antenna it is important that the tank circuit pass clear signals close to the main carrier frequency of our  $c(t)$  signal so that the transmitter achieves high signal purity and reduces interferences from unwanted frequencies. The DAC is responsible for converting the modulated signal,  $y(t)$ , back to an analog signal before transmission. If the tank circuit does not resonate close to the frequency of  $c(t)$  the DAC may incorrectly convert the digital signal resulting in dataloss within the transmitted signal. In addition to stabilizing the frequency of the AM transmitter oscillations, properly tuning the tank circuit is crucial for maximum power transfer, and impedance matching which directly impact the quality of the signal transmitted.



**Fig. 4** Diagram of tank circuit from Lab 1. The tank circuit resonates at specific frequencies, depending on the value of  $C_3$  and  $L_3$ , which directly affect signal filtering and transmission frequency. Image © 2024 Dr. Ghang-Ho Lee.

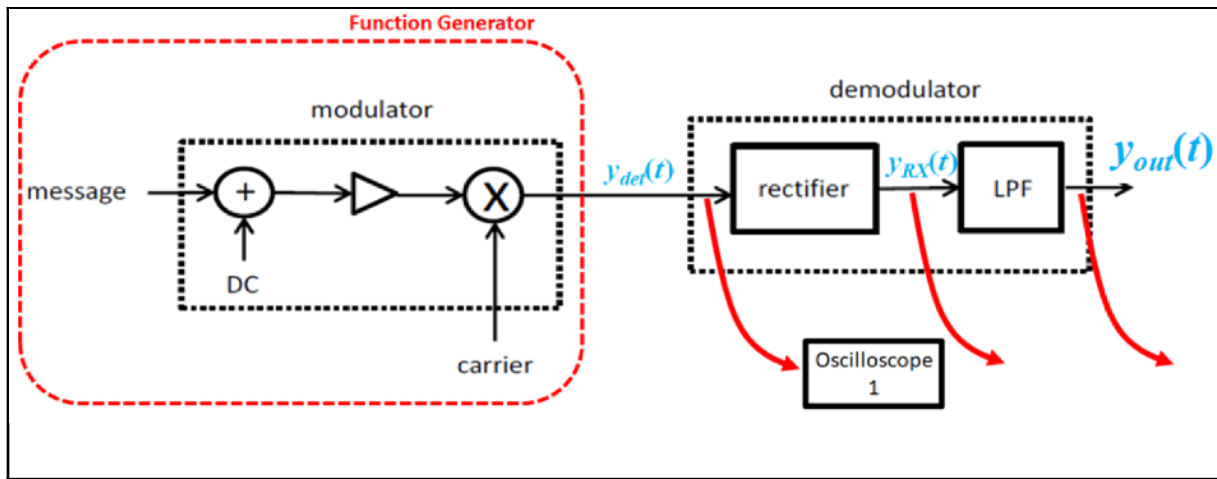


**Fig. 5** Diagram of AM modulator block from Lab 1. While you can vary inductor  $L_3$  or capacitor  $C_3$ , in Lab 1 the experiments were conducted by keeping  $L_3$  fixed and varying  $C_3$ . Image © 2024 Dr. Ghang-Ho Lee.

By effectively transferring power to the antenna the signal can efficiently propagate into the air positively impacting the range and strength of the transmitted signal. If a design doesn't ensure most of the power generated reaches the antenna, it is highly likely power will reflect back into the transmitter and dissipate as heat in the circuit. Another important feature to note about an SDR FM communication system, that is directly related to the tank circuit operation, is the highly sought after multi-mode and multi-frequency communication capabilities found in modern commercial and tactical military communication systems. By

utilizing  $L_3$  or  $C_3$  components with variability the system is able to provide this functionality to the user.

Lab 2 work is focused on the receiving and demodulating of the simulated Lab 1 signal  $y(t)$ , see Fig. 6 and 7. The demodulation phase has two main tasks: the retrieval of the message signal  $m(t)$  from the modulated signal and the removal of any remaining high frequencies from the carrier signal  $c(t)$ .

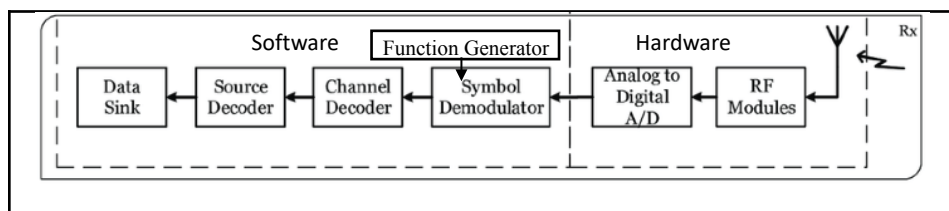


**Fig. 6** Diagram of Lab 1 AM Modulator Circuit, outlined in red dotted line, will be emulated using a function generator in Lab 2. The hardware we will construct in the AM Demodulator Circuit, Lab 2 includes an envelope and extended envelope detector see **Fig 8**. Image © 2024 Dr. Ghang-Ho Lee.

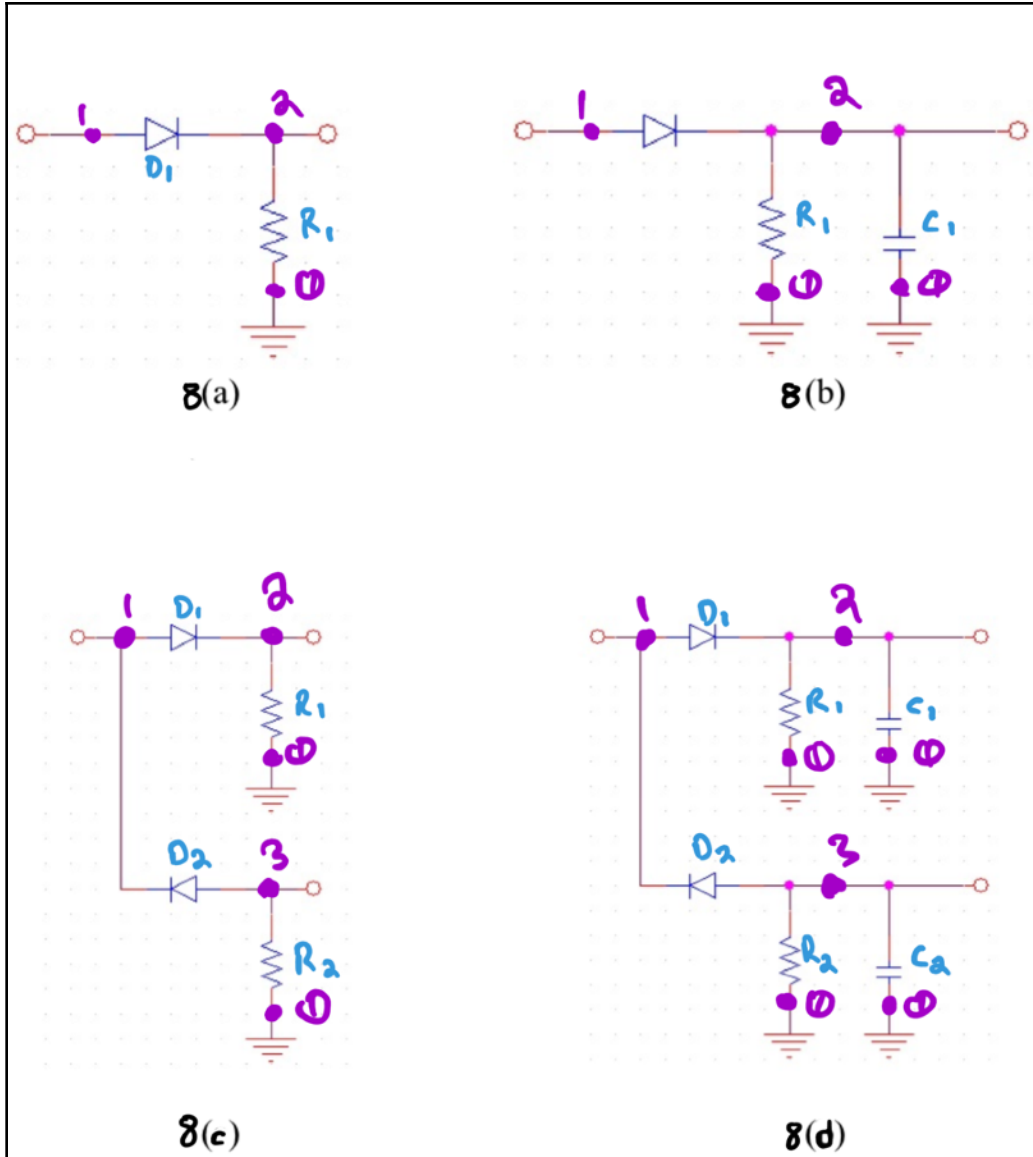
It is important to note that  $y(t)$  in Lab 1 is equal to  $y_{det}(t)$  in Lab 2. Due to limitations on our discrete parts and national broadcasting restrictions, we will simulate the transmitted signal  $y(t)$  from Lab 1 via function generator and refer to it in Lab 2 as  $y_{det}(t)$ . The general form of the  $y_{det}(t)$  equation is as follows:

$$y(t) = (A_c + m(t)) * c(t) + V_{DC\_OFFSET} \quad (1)$$

Where  $A_c = (A_m/a_{mod}) = 3$  for this portion of the communication system. For Lab 2, we explore the receiver module of a wireless communication setup and observe the effects of different analog Low Pass Filters (LPFs) by varying the  $C_1$  and  $C_2$  components presented in Fig. 8.



**Fig. 7** Block diagram of Software Defined Radio (SDR) receiver with software elements on the left, and hardware components on the right. Lab 2 leverages a function generator to implement  $y(t)=y_{det}(t)$  instead of an A/D converted signal received via antenna. Image © 2019 Hussein Kwasme & Sabit Ekin [12].



**Fig. 8** Schematic of the four circuits explored in Lab 2 with  $R_1 = R_2 = 10 \text{ [k}\Omega\text{]}$  and  $C_1 = 100 \text{ [nF]}$ . Image (a) Envelope Detector, (b) Envelope Detector with LPF tuned to a cut-off frequency of XXX [Hz], (c) Extended Envelop Detector, (d) Extended Envelope Detector with LPF tuned to a cut-off frequency of XXX [Hz]. See Fig. XXX for theoretical calculations. Netlist nodes indicated in purple. Image © 2024 Dr. Ghang-Ho Lee.

The circuits presented in Fig. 8 receive the modulated  $y_{\text{det}}(t)$  and rectify the continuous time analog signal, satisfying the first task of the AM Demodulator. Circuits presented in Fig. 8b and 8d satisfy the second task of the AM Demodulator of filtering out the higher frequency of the carrier signal  $c(t)$ . This filtering is implemented using the capacitors  $C_1$  and  $C_2$  in parallel with  $R_1$  and  $R_2$  denoted as  $\tau_1$  and  $\tau_2$ . It is essential to find the cut-off frequency using the formula:

$$f_{\text{CUT\_OFF}} = (1/(2\pi R_i C_i)) \quad (2)$$

Where  $i = \{1,2\}$  for fully rectified circuits, Fig 8c. and 8d. We can determine the exact capacitance required to complete a capacitor's charge/discharge cycle so that it closely follows our message signal envelope and removes higher frequencies associated with the carrier signal  $c(t)$ . Lab 2 ends after this demodulation stage, but future work towards implementing the entire communication system would include implementing the coder in the transmitter and decoder in the receiver stages. Calculations to determine the filtering frequencies are presented in the next section; see Fig. XXX. By completing Lab 1, we have implemented workflows for generating, modulating, and transmitting a communication signal. In Lab 2, we have implemented workflows for receiving and demodulating these signals. Several calculations are essential to LPF design and are presented in the following section, such as determining the attenuation of frequencies associated with the carrier frequency  $c(t)$ .

## 2. Calculations

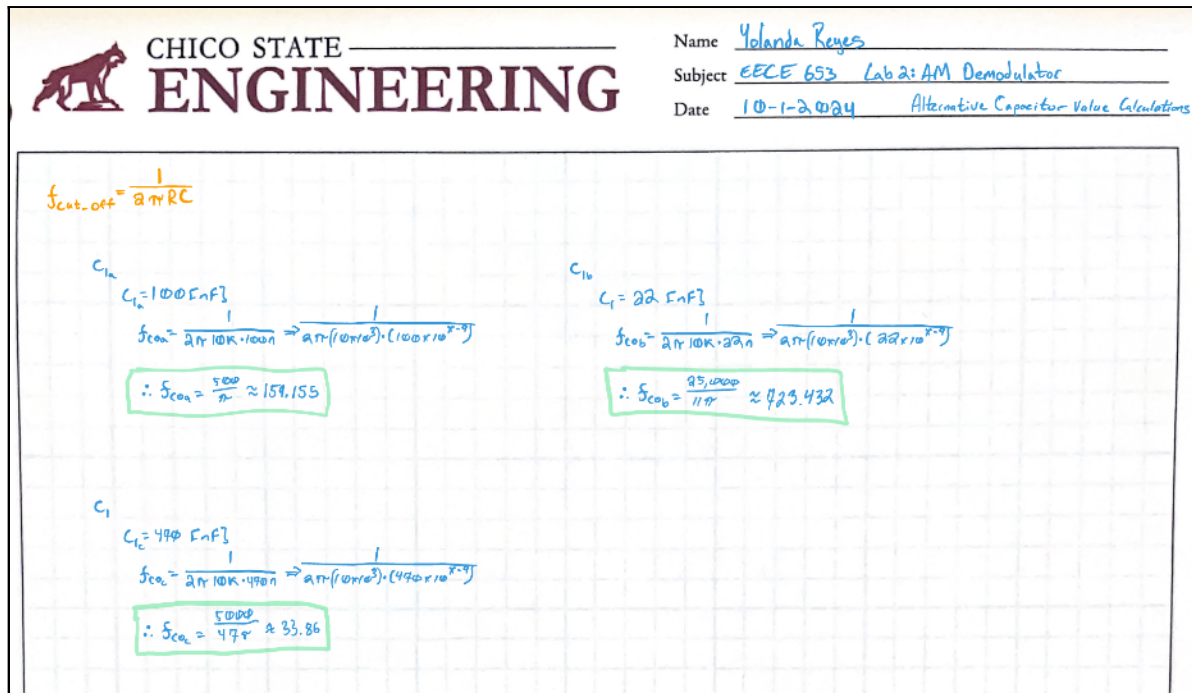
### 2.1. Filter Design based on Calculations for Time Constants $\tau_1$ and $\tau_2$

To implement the Lab 2 AM receiver demodulator, we start by performing calculations (see Fig. 9) to determine the RC time constants,  $\tau_1$  and  $\tau_2$ , and the cut-off frequency of the Extended Envelope Detector with Low Pass Filter circuit (see Fig 8d).

|  |   |
|--|---|
| $\text{cut-off frequency: } f_{\text{cut-off}} = \frac{1}{2\pi RC}$ $f_{\text{c}} = \frac{1}{2\pi RC} \quad \text{Solve for } C$ $C \cdot f_{\text{c}} = \frac{1}{2\pi R}$ $C = \frac{1}{2\pi R f_{\text{c}}} \Rightarrow C = \frac{1}{2\pi R f_{\text{c}}} \quad \text{Assume } 300 \text{ Hz} = f_{\text{c}}$ $C = \frac{1}{2\pi \cdot 10k \cdot 300} \therefore C = 5.30516 \times 10^{-8} \text{ F}$ $C = 53.0516 \text{ nF}$ <p style="text-align: center;">2b.</p> | <p><b>Fig. 9</b> Calculation for determining the values of capacitors to use during the experiment portion of Lab 2. The message <math>m(t)</math> signal is operating at 100 [Hz] and so the cut-off frequency was assumed to be 300 [Hz]. Image © 2024 Yolanda Reyes.</p> |
|--|---|

The calculations for the first part of the analysis for Lab 2 are essential because by determining the time constant  $\tau$ , we gain insight into how the filter will operate to provide the feature of an intended cut-off frequency of 300 [Hz]. By determining where the message portion of the  $y_{\text{det}}(t)$  signal will be in the received signal, an effectively designed filter will remove the higher frequencies associated with the carrier signal  $c(t)$  portion of  $y_{\text{det}}(t)$ . By taking the Z-Transform of the time domain equation analysis can utilize the location of the poles, an indicator of system stability, and zeros, which provide control over performance features such as elimination of unwanted frequencies in  $y_{\text{det}}(t)$  to meet design

parameters when applying these concepts to real-world applications. Due to the availability of parts to meet these initial values, several replacements for  $C_1$  and  $C_2$  were calculated and used in the experiment portion of this report (see Fig 10).



**Fig. 10** Re-calculating values for potential capacitors to use in the experimental circuit implementation presented in the experimental portion of this report, see pp. XXX. By selecting 22 [nF], 100 [nF], and 470 [nF] values for the circuit presented in **Fig. 8d** we remove specific frequencies from the signal presented in **Fig. XXX** and tune the filter of the system. It is also important to note that the frequency variable in the discrete time domain is unit-less.

Image © 2024 Yolanda Reyes.

The receiver's demodulating component is tuned according to the calculations presented in Fig. 10 with results being discussed in Section 5 Results and Conclusion. will be presented in the experiment and results portion of this report (see pp. XXX). To further analyze the demodulator's expected behavior, the Z-Transform of the time-domain equation is leveraged to determine the side lobes of the message signal  $m(t)$  portion contained in the  $y_{out}(t)$  signal in Fig. 6.

## 2.2. Time domain to Z-Domain Transformation

Analysis in the Z-Domain enables the assessment of the frequency response. It is one of the critical features system designers must consider when determining how to modulate and transmit, as well as receive and demodulate signals. Theoretical calculations for the expected spectrum analyzer output during experiments, according to the Fig. 11, are presented in Fig. 12.

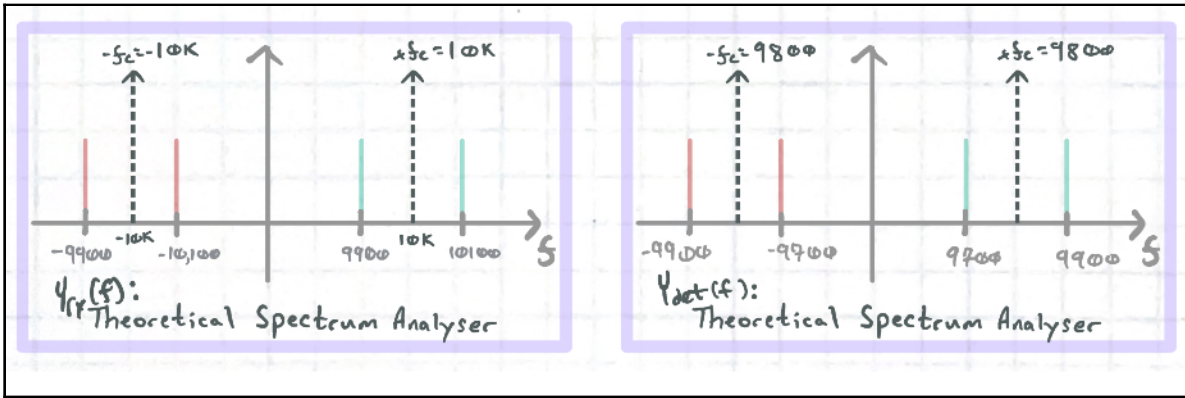


Fig. 11 Calculating side-lobes of  $y_{\text{det}}(f)$ , an  $y_{\text{rx}}(f)$ . This is the region of the  $y_{\text{det}}(t)$  where data is present and would require further processing in the decoder portion of the system, see Fig. 6 and Fig. 7. Image © 2024 Yolanda Reyes.

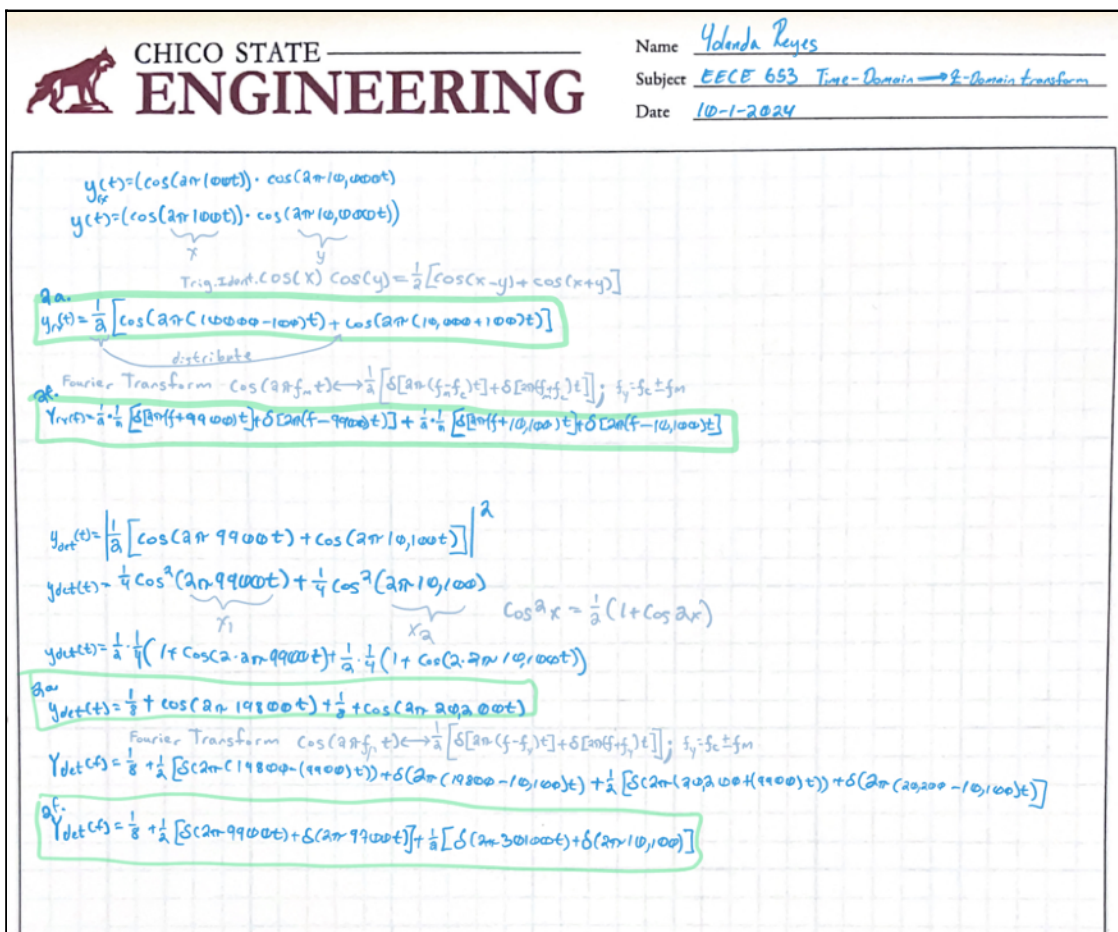


Fig. 12 Calculating the mathematical representation of the modulated signal  $y(t)$ , which is a carrier signal  $c(t)$  multiplied by a message signal  $m(t)$  represented in Lab 2 as  $y_{\text{rx}}$  and  $y_{\text{det}}$ , see Fig. 7. Image © 2024 Yolanda Reyes.

From the calculations of the Z-Domain Transform, the theoretical calculations present us with the following results, which are discussed further with experimental values in Section 4. Experimental Results (see pp. XXX). The general mathematical model for representing  $y_{\text{det}}(f)$  and  $y_{\text{rx}}(f)$  takes the form:

$$Y_{\text{det}}(f) = \delta(n_{\text{det}}) + \delta(n_{\text{det}}-1) + \delta(n_{\text{det}}-2) + \dots + \delta(n_{\text{det}}-k) \quad (3)$$

$$Y_{\text{rx}}(f) = \delta(n_{\text{rx}}) + \delta(n_{\text{rx}}-1) + \delta(n_{\text{rx}}-2) + \dots + \delta(n_{\text{rx}}-k) \quad (4)$$

The delta  $\delta$  terms indicate when the experiment should yield spikes in the frequency, which include four calculations but only three unique frequency values of 9700, 9900, and 10100, presented Fig. 12.

### 2.3. Envelope Detector: Rectifier Only

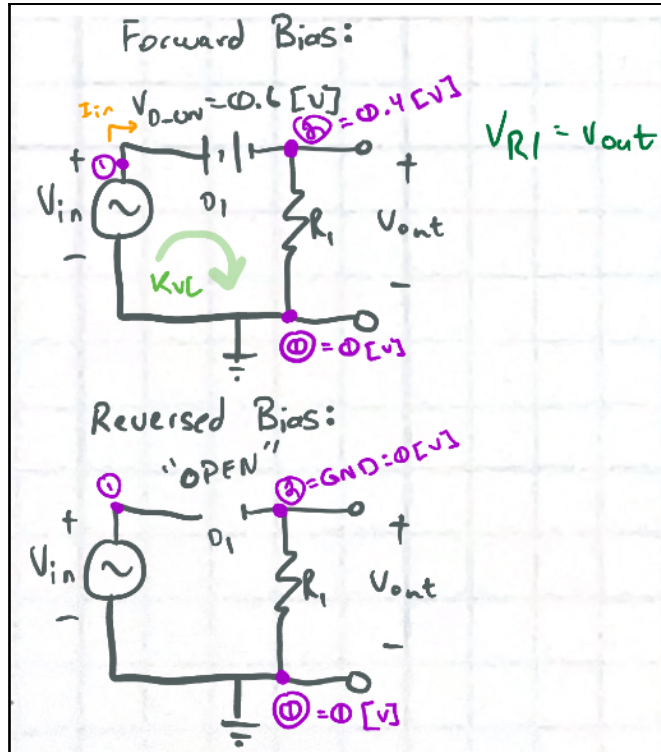


Fig. 13 The half wave rectifier envelope detector circuit in forward and reversed bias. Netlist nodes indicated in purple. Image © 2024 Yolanda Reyes.

The equivalent circuit for a half-wave rectifier, first presented in Fig. 8a circuit, can filter the positive portion of the AC signal. It is important to note that this signal still requires further processing but provides the opportunity to observe how the voltage drops across the load and derive an equation for  $V_{\text{out}}$ , see Fig. 13.

With this information, the next step is to derive the equation (5) for the expected value of  $V_{\text{out}}$ . Using the datasheet for N4148 fast-switching diode, see page XXX, it is determined that the voltage required to turn on the diode will be 0.6 [v]. Therefore, in forward bias, the voltage out to the decoding portion of the communication system can be represented by the equation:

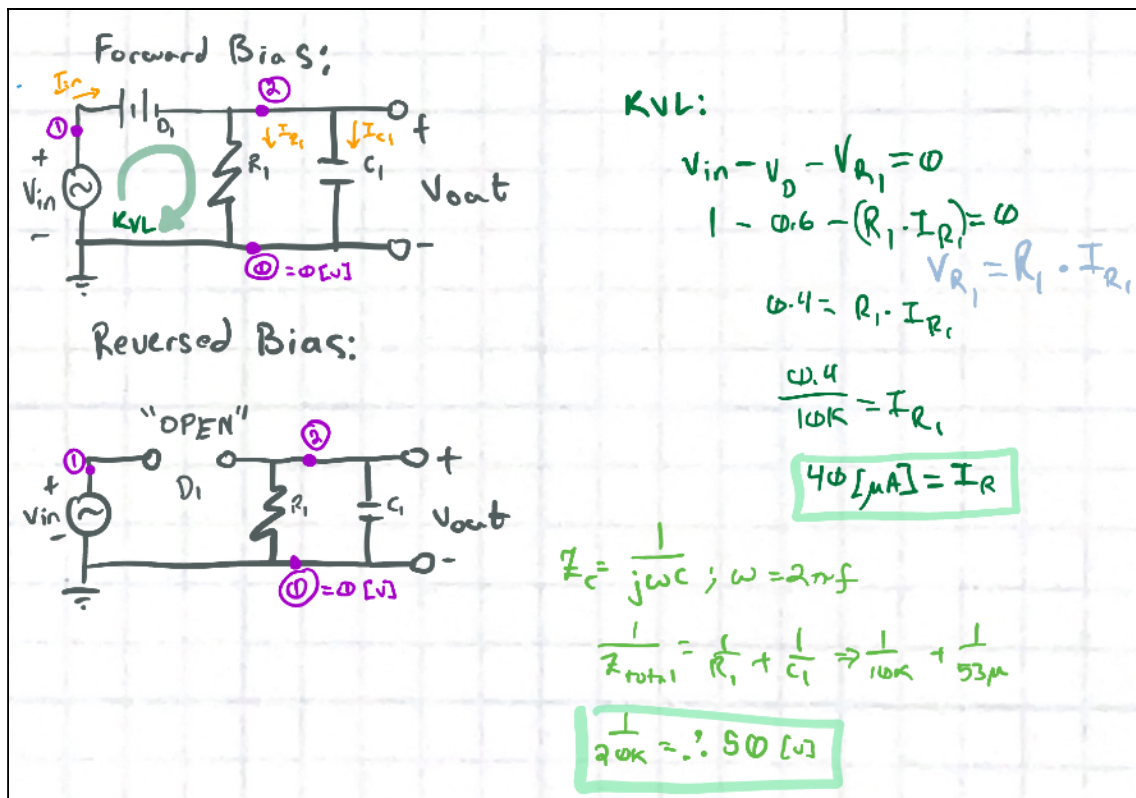
$$V_{\text{out}} = V_{\text{in}} - 0.6 \text{ [v]} \quad (5)$$

With the amplitude of the signal  $y_{det}(t)$  reaching a max voltage of 1.5, we expect to get a range of voltage drops over  $R_1$  from  $0.6 [v] < V_{in} < 0.9 [v]$ . When  $V_{in} < 0.6 [v]$ , the circuit in Fig. 13 is in reversed bias, and GND is connected to  $V_{out}$ , which is equal to  $V_{R1}$ , resulting in  $y_{rx}(t) = 0$  during the negative portion of the AC signal  $y_{det}(t)$ . The  $y_{rx}(t)$  signal needs to be tuned to reduce ripple. The frequency calculations presented in Fig. 10 are the values to be implemented during the experiment portion of Lab 2.

## 2.4. Envelope Detector: Rectifier and LPF

Extended signal tuning capabilities are acquired with a capacitor  $C_1$  added in parallel to  $R_1$  (see Fig. 8b). One of the primary purposes of including the capacitor  $C_1$  is to use equation (2) to determine where to cut off the higher frequencies associated with the carrier signal  $c(t)$ , that are still present in the half-wave rectified signal  $y_{rx}(t)$  (see Fig. 6) is one of the main purposes of including the capacitor  $C_1$ .

The goal of the demodulator circuit is to eventually reconstruct the message signal  $m(t)$  data once the higher-frequency carrier signals are filtered out. The circuit presented in Fig. 14 contains half of the information required to send the signal to the decoder portion of the system. Resolving the negative cycle of the signal  $y_{det}(t)$  requires an upgrade from a half-wave rectified signal to a full-wave rectified signal.



**Fig. 14** The half-wave rectifier envelope detector with Low Pass Filter (LPF) circuit in forward and reversed bias. Depending on the  $\tau_1$ , time constant value of  $R_1$  and  $C_1$ , the response will be tunable to specific frequencies, blocking those associated with the carrier signal  $c(t)$  portion of the  $y_{rx}(t)$ . Netlist nodes indicated in purple. Image © 2024 Yolanda Reyes.

## 2.5 Extended Envelope Detector: Rectifier Only

The extended envelope detector requires a full-wave rectifier to capture the entire  $y_{det}(t)$  AM signal. Capturing the entire signal is crucial because, in the decoder phase, peak-to-peak voltage is used to determine what binary code to extract from the signal. In Fig. 15, the Extended Envelope Detector, full-wave rectifier equivalent circuit is presented, showcasing Kirchhoff's Voltage Law (KVL) equations for the expected value of  $V_{out}$  in the circuit presented in Fig. 8c.

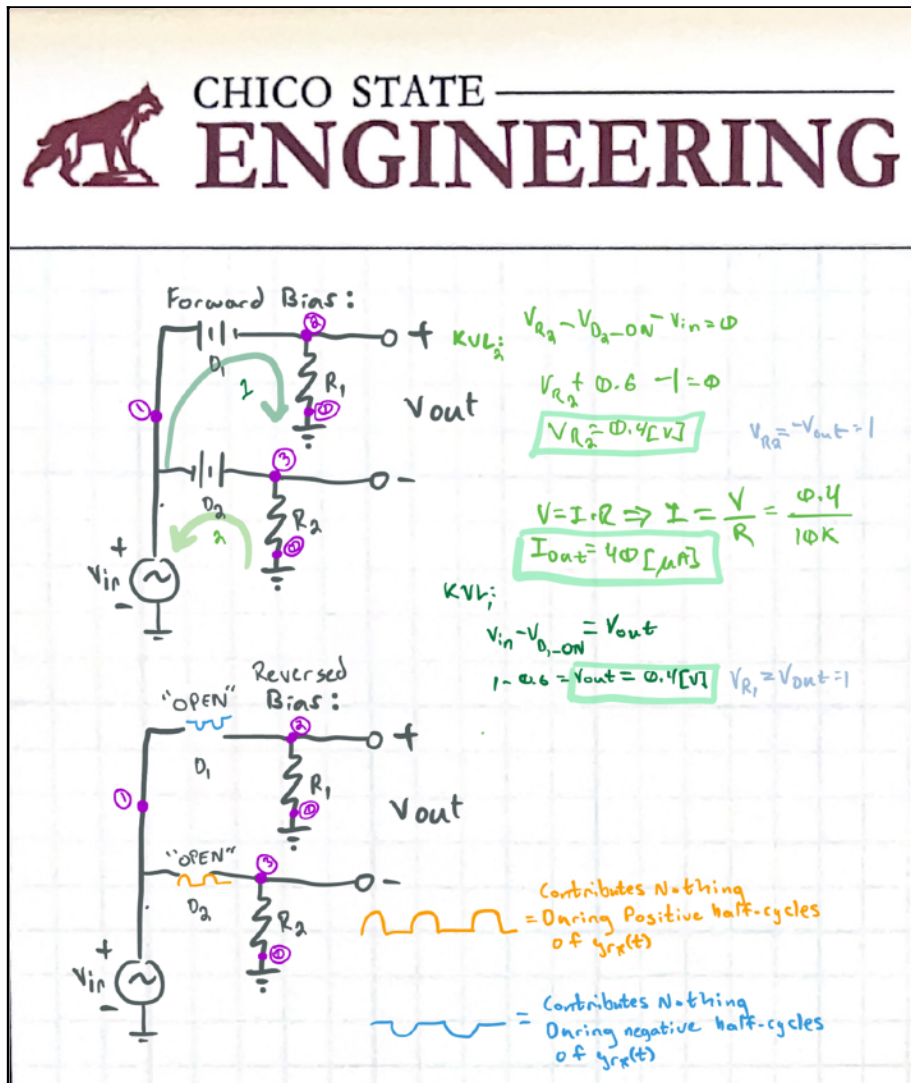


Fig. 15 Extended Envelope Detector, full-wave rectifier only. This circuit enables for the full wave to be rectified since the addition of  $D_2$  and  $R_2$  now drive  $V_{out}$  during the negative half cycle of  $V_{in}$  which is equal to the negative half cycle of  $y_{det}(t)$ . Image © 2024 Yolanda Reyes.

The forward or reverse bias case illustrated in Fig. 15 is essential to take note of because depending on the polarity of the signal  $V_{in}$ , D<sub>1</sub> and D<sub>2</sub> will either be in forward or reverse biased capturing the envelope of the entire AM signal  $y_{det}(t)$ , completing task one of a demodulator circuit. The second task of a demodulator is determining where to implement filtering, such as Low Pass and Band Pass, and at what specific frequencies or ranges of frequencies is the next concern. Filtering out the carrier signal  $c(t)$  portion of the  $y_{rx}(t)$  signal provides a refined  $y_{out}(t)$  ready for decoder modules in the overall communication system.

## 2.6 Extended Envelope Detector: Rectifier and LPF

The circuit presented in Fig. 8d is redrawn in Fig. 16 to analyze the forward and reversed biased behavior of the Extended Envelope Detector with a Low-Pass Filter. This circuit configuration is designed to remove higher frequencies associated with the carrier signal  $c(t)$  portion of  $y_{rx}(t)$  in both the negative and positive half-cycles of  $V_{in}$ . At this point in the analysis, the design satisfies the two main tasks for an AM Demodulator system.

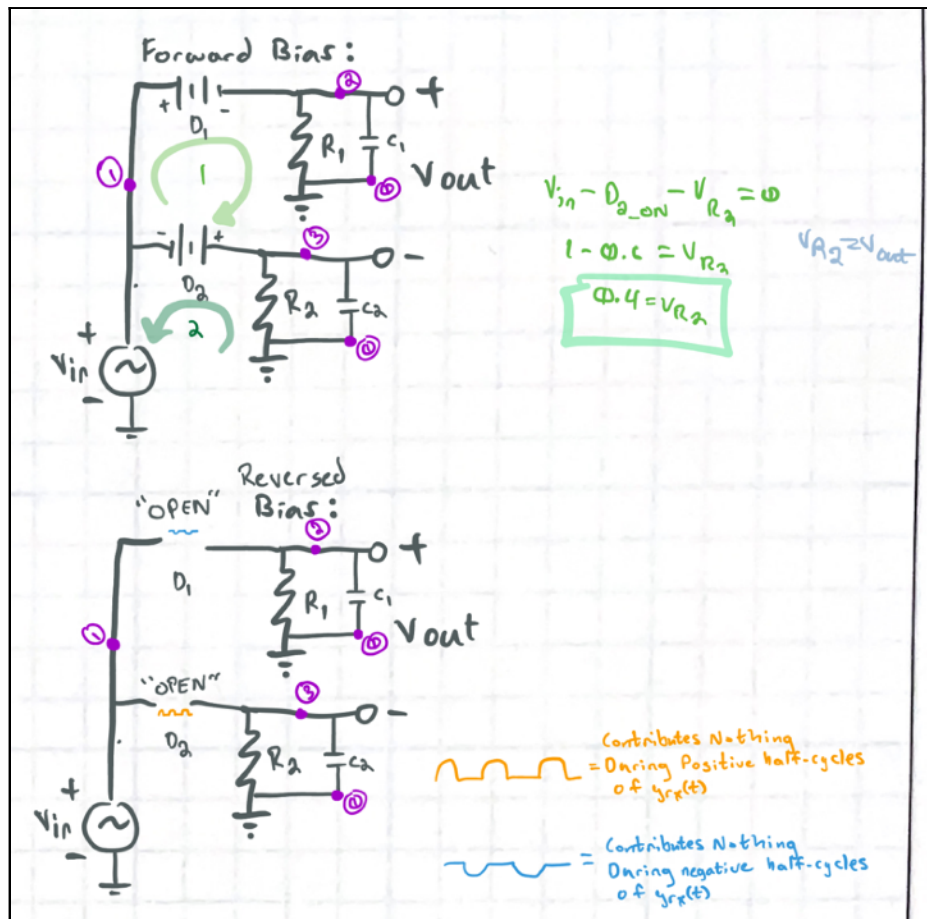


Fig. 16 The Extended Envelope Detector with LPF implemented by adding C<sub>1</sub> and C<sub>2</sub>. These two capacitors varied in capacitance during the experiment. took on values of 22 [nF], 100 [nF], and 470 [nF]. By tuning  $y_{out}(t)$  in this way observations can be made about the behavior of optimizing for digital cut-off frequencies of 33.86, 159.155, and 723.432 (see Fig. 10).

With a theoretical understanding of the demodulator circuit, an interesting question is, what peak-to-peak voltage range would trigger the system to send a logic low or logic high value to the next stage in the communication system? At this stage, the communication system transmits binary 0s and 1s to the channel and source decoder modules. In these modules, the system can begin mapping out what the message signal  $m(t)$  communicated. For Lab 2, the main goal is to observe the effect of different filtering and cut-off frequencies on a system's ability to extract a message from a modulated signal that includes a carrier frequency. In the next section, several simulations in MATLAB and LtSPICE provide more information on variables of interest to observe during the experimental portion of Lab 2, AM Demodulator.

### 3. Simulations

#### 3.1. MATLAB

To run MATLAB simulations for spectrum analyzer output, the fully rectified extended envelope detector,  $y_{rx}$ , signal  $m(t)$ , and carrier signal,  $c(t)$ , must be represented in the time domain. The first step is to utilize the trigonometry identity to generalize the output signal  $y(t)$ :

$$\cos^2(\theta) = 1/2 [1 + \cos(2\theta)] \quad (6)$$

In MATLAB, our goal was to simulate the expected output,  $y_{det}(t)$ , over time, and the frequency-domain spectrum analyzer output for different message signal frequencies. With equation (16) calculated, the Fourier Transform of this equation is required to complete this process and analyze output in the frequency domain:

$$\cos(2\pi*f_m*t) \Rightarrow (1/2) [\delta[2\pi*(f-f_m)*t] + \delta[2\pi*(f+f_m)*t]] \quad (7)$$

Theoretical spectrum analyzer traces, calculated in Fig. 11 and 12, are confirmed in simulations performed for MATLAB. In the output, the sidebands represent the actual message signal,  $m(t)$ , data. The carrier signal,  $c(t)$ , carries the lower-frequency  $m(t)$  signal so it can be transmitted efficiently over a higher frequency band. Transmitting over a higher frequency helps reduce noise and interference, significantly affecting lower-frequency bands.

Analyzing the sidebands presented as peaks in the MATLAB simulations also presents information about the transmission bandwidth. The foundational code provided by Dr. Lee is utilized as a starting point, and the equations for  $y_{rx}$  assume several cut-off frequencies will be observed with calculated values of 33.86, 159.155, and 723.432 (see Fig. 10).

Current Folder

|                                 |
|---------------------------------|
| Lab2_AM_Demodulator.m           |
| Lab2_AM_Demodulation_FFT_Ref_.m |
| Fig4b.op.raw                    |
| Fig4b.cir                       |
| Fig4a.op.raw                    |
| Fig4a.cir                       |
| Fig3b.op.raw                    |
| Fig3b.cir                       |
| Fig3a.op.raw                    |
| Fig3a.cir                       |
| Fig2.op.raw                     |
| Fig2.log                        |
| EECE 653 Lab 2.pages            |

Editor - /Users/scholar/Desktop/Chico State/Fall 2024/EECE 653/Lab 2 AM Demodulator/Lab2\_AM\_De...

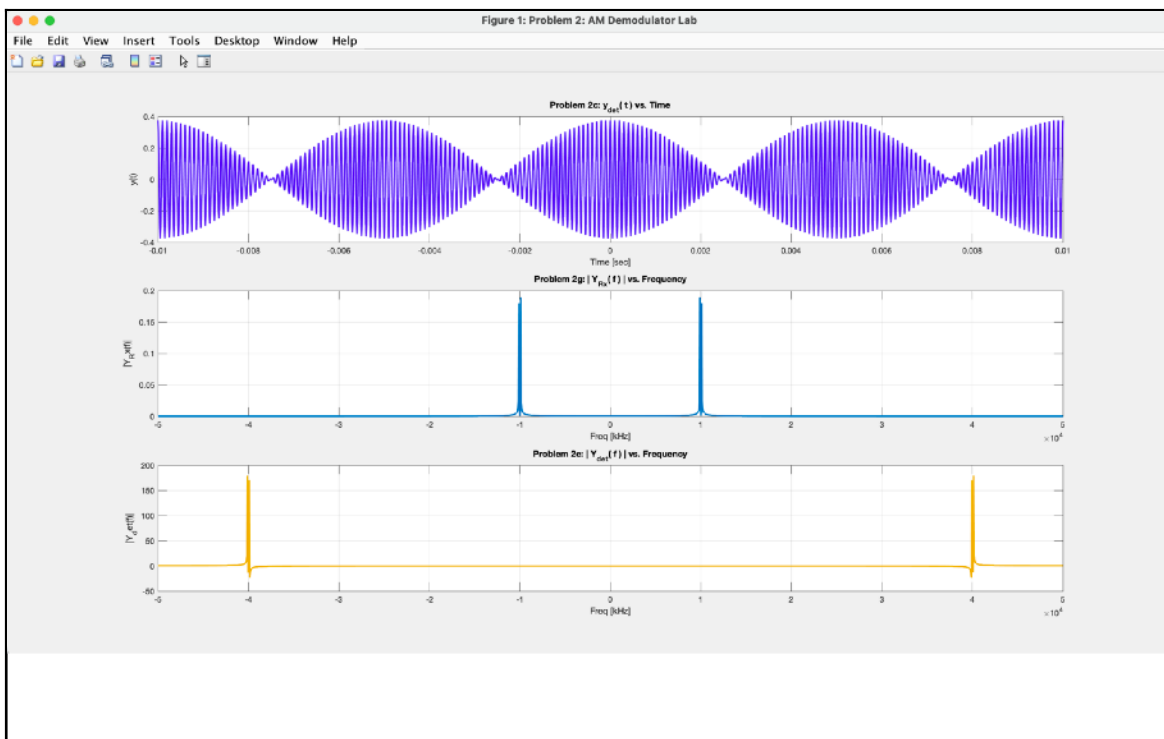
```
% Name %
Lab2_AM_Demodulator.m + %
1 % Lab 2 Preparation MATLAB HW
2 % Yolice Reyes 9/29/2024
3 % EECE 653 Software Defined Radio
4 %
5 % ***** Problem 2c, 2E, and 2g *****
6 clear all; close all; % Time variable from 0 - 0.02 [seconds], step size 10 [microseconds]
7 T = 0.02; % defining time RANGE
8 Ts = 0.00001; % defining time STEP SIZE
9 tm = -T/2:T*1/T; % defining time array, from -0.01 - 0.01 [seconds]
10 Ac = 1.5; % Modulation index
11 omega = pi/3; % Carrier frequency
12 mcos = 0.2*cos(2*pi*tm); % Message signal as = 0.2 [0-10], f = 100 [Hz]
13 et = 1.5*cos((2*pi*omega*tm)); % Carrier signal Ac = 3 [0-10], f = infinite
14 yt = mcos.*et; % Modulated signal, at center towards carrier freq. with sidebands qz/- 9900 [Hz] & 101 [kHz]
15 %Wd = cos(2*pi*f.*1000000).wm; % AM representation without DC offset
16 %
17 F = 3/Ts; % defining frequency RANGE from time STEP SIZE
18 fs = 1/T; % defining frequency STEP SIZE from frequency RANGE
19 fn = 0:fTs; % defining frequency array
20 fm_1 = fn-F/2; % defining frequency array (zero at center)
21 fm_2 = fn+F/2;
22 %
23 Ys = fft(yt); % Perform FFT to find frequency domain signal
24 L_Ys = length(Ys); % Measuring length of Ys to perform AMPLITUDE NORMALIZATION
25 %
26 Ys_2 = fftshift(Ys)/L_Ys/2; % FFTSHIFT and AMPLITUDE NORMALIZATION
27 %
28 figure('Name','Problem 2: AM Demodulator Lab')
29 %
30 % *****|Y(t)| vs Time *****
31 subplot(1,1,1), plot(tm, yt, 'LineWidth',2,'Color',[0.3010 0.1458 0.9330]), % Color: [0.3010 0.1458 0.9330]
32 grid on; xlabel('Time [sec]'); ylabel('y(t)');
33 title('Problem 2c | Y_d_m(t) | vs. Time');
34 %
35 %
36 % *****|Y(t)| vs Frequency *****
37 subplot(1,1,2), plot(tm, abs(Ys), 'LineWidth',2,'Color',[0.4470 0.7410]), % Color: [0.4470 0.7410]
38 grid on; xlabel('Freq [MHz]'); ylabel('|Y(t)|');
39 title('Problem 2c | Y_d_m(t) | vs. Frequency');
40 %
41 %
42 %
43 %
44 %
45 % *****|Y_d_e(t)| vs Frequency *****
46 subplot(1,1,3), plot(tm,2, abs(Ys_2), 'LineWidth',2,'Color',[0.9290 0.6940 0.1250]), % Color: [0.9290 0.6940 0.1250]
47 grid on; xlabel('Freq [MHz]'); ylabel('|Y_d_e(t)|');
48 title('Problem 2e | Y_d_e(t) | vs. Frequency');
49 %
50 %
51 % There are several things to take note of after performing the theoretical calculations. The PATHLOSS of the output. Calculations need to be confirmed should there be three spikes in the Frequency plot. If the spikes are supposed to be 3 or two. If there are three spikes, +-9900, -9700, & +-10,100. In the experiment then I would then look to the Gaussian plot for further clarity of the results. We do know the data of the received signal will be in the side lobes and the carrier frequency would be the highest peak in the Gaussian plot.
52 %
53 %
54 %
55 %
56 %
57 %
58 %
59 %
60 %
```

Select a file to view details

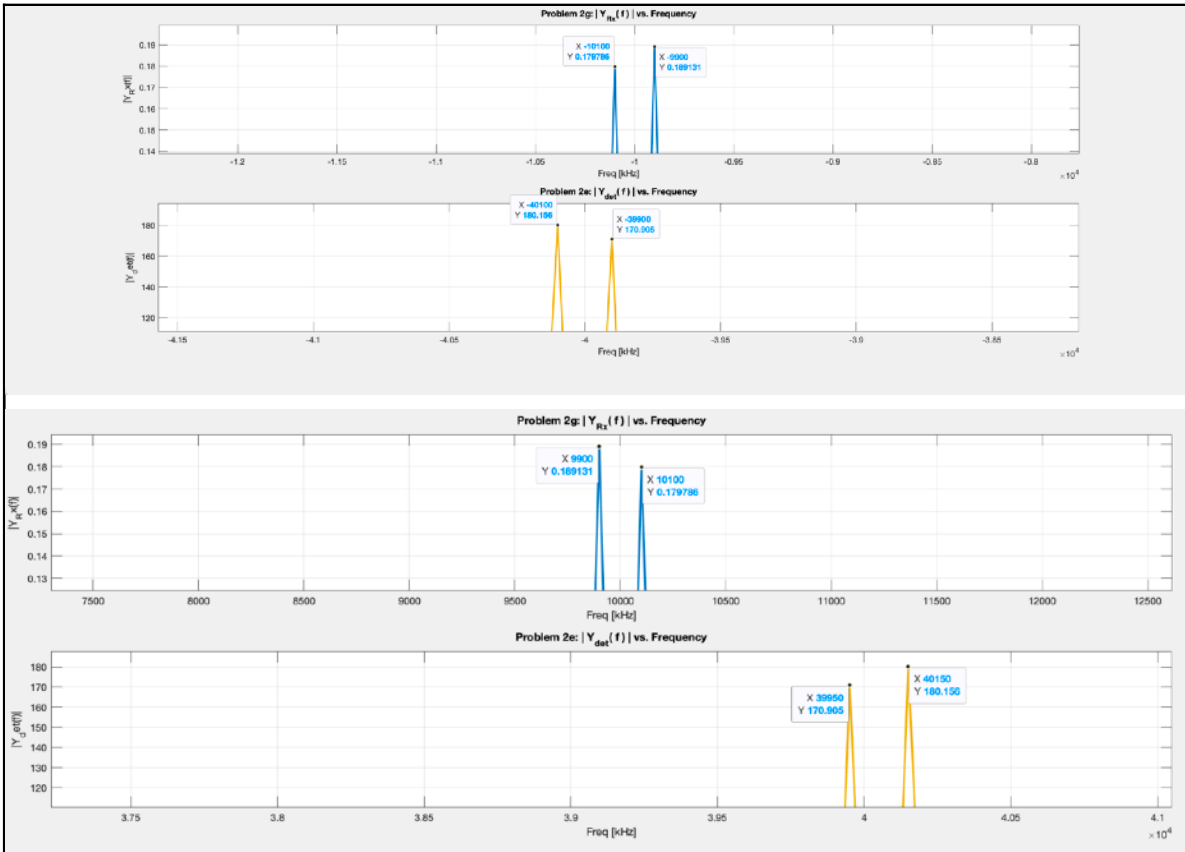
Workspace

|        |                    |
|--------|--------------------|
| Name % | Value              |
| Ac     | 1.5000             |
| amod   | 0.1667             |
| ct     | 1.0000e+05         |
| F      | 1x2001 double      |
| fn     | 1x2001 double      |
| fn_2   | 1x2001 double      |
| Fs     | 50                 |
| L_Ys   | 2001               |
| mt     | 1x2001 double      |
| T      | 0.0200             |
| tn     | 1x2001 double      |
| Ts     | 1.0000e-05         |
| Ys     | 1x2001 complex ... |
| Ys_2   | 1x2001 complex ... |
| yl     | 1x2001 double      |

**Fig. 17** MATLAB source code for plotting the  $y_{det}(t)$  vs. Time,  $|Y_{Rx}(f)|$  vs. Frequency, and  $|Y_{det}(f)|$  vs. Frequency. the output of the plots are presented in **Fig. 18**. Image © 2024 Yolanda Reyes.



**Fig. 18** MATLAB plots from source code presented in **Fig. 17**. The source code for Problem 2c presents plots for  $y_{\text{det}}(t)$  vs. Time in purple on top,  $|Y_{\text{Rx}}(f)|$  vs. Frequency in blue in the middle, and  $|Y_{\text{det}}(f)|$  vs. Frequency in orange on the bottom. Image © 2024 Yolanda Reyes.

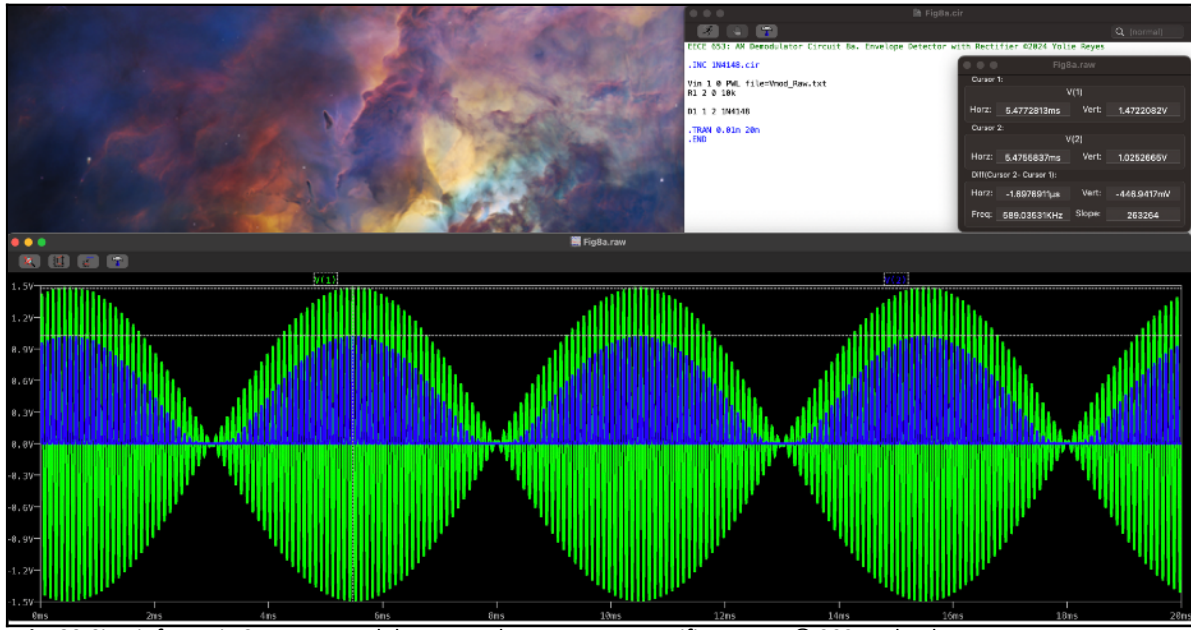


**Fig. 19** MATLAB plots zoomed in to view peaks of interest. On top the negative frequencies, on bottom the positive frequencies. The simulated frequencies in blue confirm what was theoretically calculated in the previous section presented in **Fig. 11 - 12**. Image © 2024 Yolanda Reyes.

Completing the MATLAB simulations requires consideration of the meaning of the orange plots of the square law detector  $y_{det}(t)$  signal in the orange plots in Fig. 18 and 19 and the value for  $Y_{det}(f)$  calculated in Fig. 11 and 12, where calculated to be present with spikes at -9700 and -9700, see Section 5, Results and Conclusion pp. XXX. While the MATLAB simulations present some insight into the frequencies we can expect from our  $y_{out}(t)$  signal after filtering, simulations on expected voltages can also be carried out for other purposes, such as determining if the received signal is to send binary low 0s or binary high 1s.

### 3.2. LtSPICE: $V_{out}$ vs. $V_{in}$

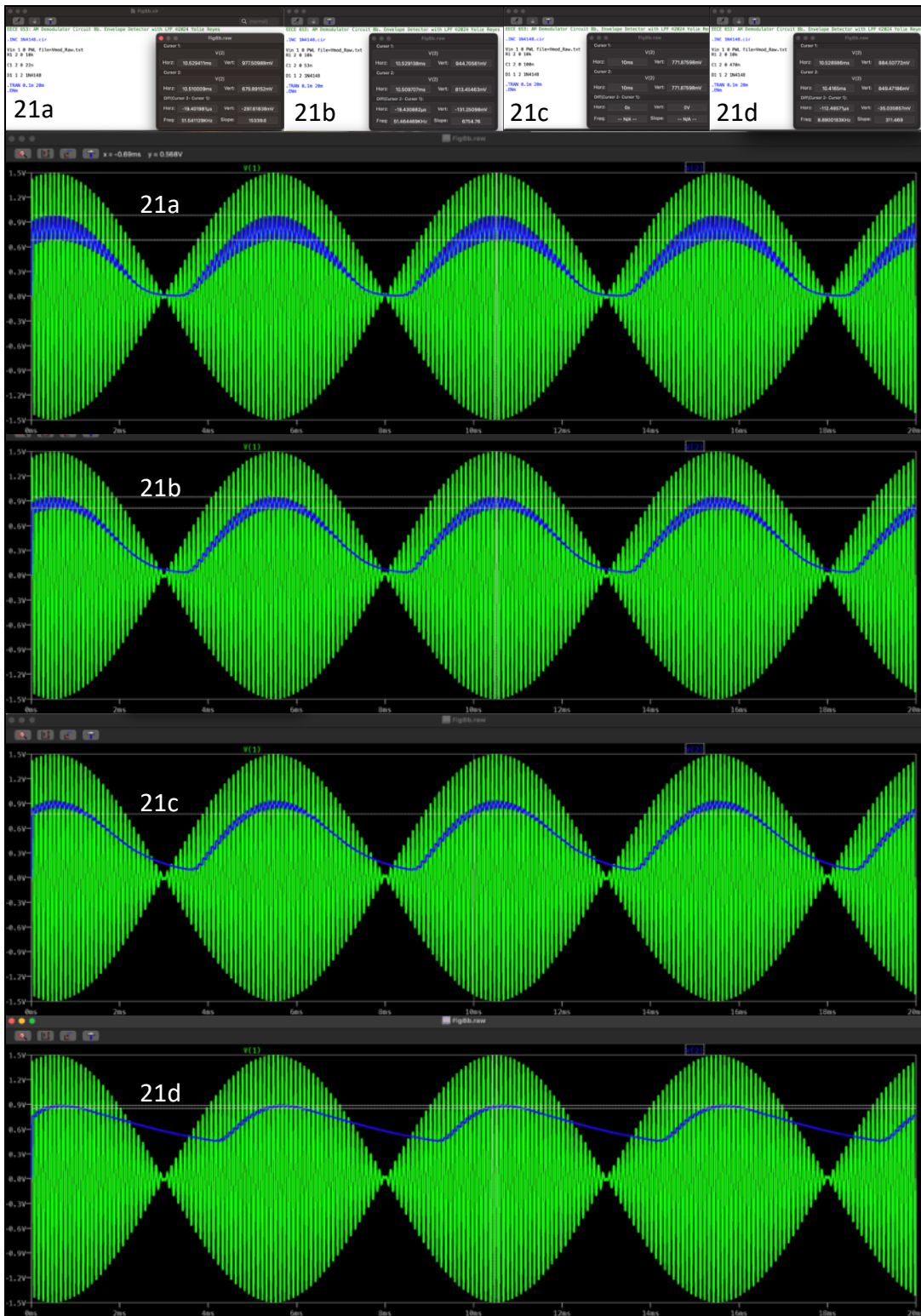
The signals are digitally represented as 0s and 1s in a digital system. Establishing threshold voltage ranges sends a demodulated signal to the decoders as a series of 0s and 1s ready to be decoded. LtSPICE simulations give preliminary information on the expected voltage range for what will be interpreted as 0s and 1s in the digital system. The following section, evaluates several different capacitors for  $y_{out}(t)$  signal quality. Factors such as attenuation, aliasing, and clipping of the signal  $y_{rx}(t)$  as it travels through the envelope detector and out of the LPF portion of the circuit design are presented in Fig. 20 and 21.



**Fig. 20** Circuit from Fig 8a AM Demodulator: Envelope Detector Rectifier. Image © 2024 Yolanda Reyes.

In Fig. 20, we see a simulation of the expected output of an envelope detector,  $y_{rx}(t)$ . There are still portions of the carrier signal  $c(t)$  in the  $y_{det}(t)$  and  $y_{rx}(t)$ .  $y_{det}(t)$  is presented in green, while  $y_{rx}(t)$  is presented in blue. AM Demodulator design aims to detect the envelope and remove the carrier signal. By varying the time constant  $\tau_1$ , the charge/discharge cycle of the RC circuit is tuned to attenuate specific frequencies.

In Fig. 21, several behavior plots of  $V_{in}$  vs.  $V_{out}$  were created, and simulations were run on four scenarios: 21a.  $C_1 = 22$  [nF], 21b.  $C_1 = 53$  [nF], 21c.  $C_1 = 100$  [nF], 21d.  $C_1 = 470$  [nF]. Analysis of the LPF effects on the signal presents several options for stable system consideration, 21a and 21b. In signals 21a and 21b, the attenuation level may be acceptable; however in 21c and 21d, the signal is getting distorted and will probably result in data loss and instability. By running similar LtSPICE simulations on the circuits presented in Fig. 8c and 8d, we get a clearer picture of the capabilities of a fully designed system implemented in the lab.



**Fig. 21** LtSPICE simulations for circuits from Fig 8b AM Demodulator: Envelope Detector Rectifier with LPF.  $C_1 = \{22, 53, 100, 470\}$  [nF]. This part of the design is responsible for filtering just the message  $m(t)$  signal portion, plotted in blue, of  $y_{rx}(t)$ . By removing higher frequencies we are filtering out the carrier  $c(t)$  signal portion of the  $y_{rx}(t)$  signal received and which is plotted in green. Careful consideration for the filter is important to reduce attenuation of the signal and loss of data. Several filtering options are simulated 21a.  $C_1 = 22$  [nF], 21b.  $C_1 = 53$  [nF], 21c.  $C_1 = 100$  [nF], 21d.  $C_1 = 470$  [nF] Image © 2024 Yolanda Reyes.

The Extended Envelope Detector circuit from Fig. 8c enables rectifying the full signal  $y_{det}(t)$ . By rectifying the whole signal, efficiency is improved by utilizing both half-cycles of an AM signal. Using both half-cycles provides access to a design with a better response to signal changes. Since AM communication applications utilize variations in amplitude as the protocol followed to encode data, an excellent response to signal changes is a crucial feature to consider for a reliable AM Demodulator for Lab 2. In Fig. 22, the LtSPICE plot presents us with a well detected envelope with high-frequency filtering,  $y_{out}(t)$ , composed of the positive half cycle in the dark blue, negative half cycle in teal, original AM Modulated signal,  $y_{det}(t)$ , provided by function generator in green.

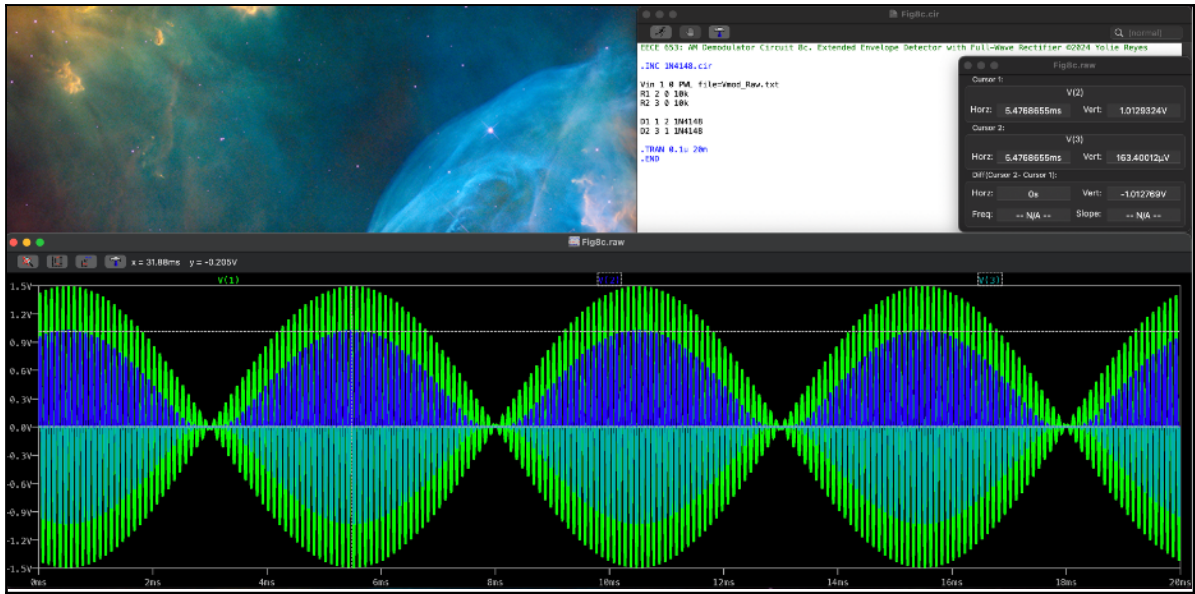
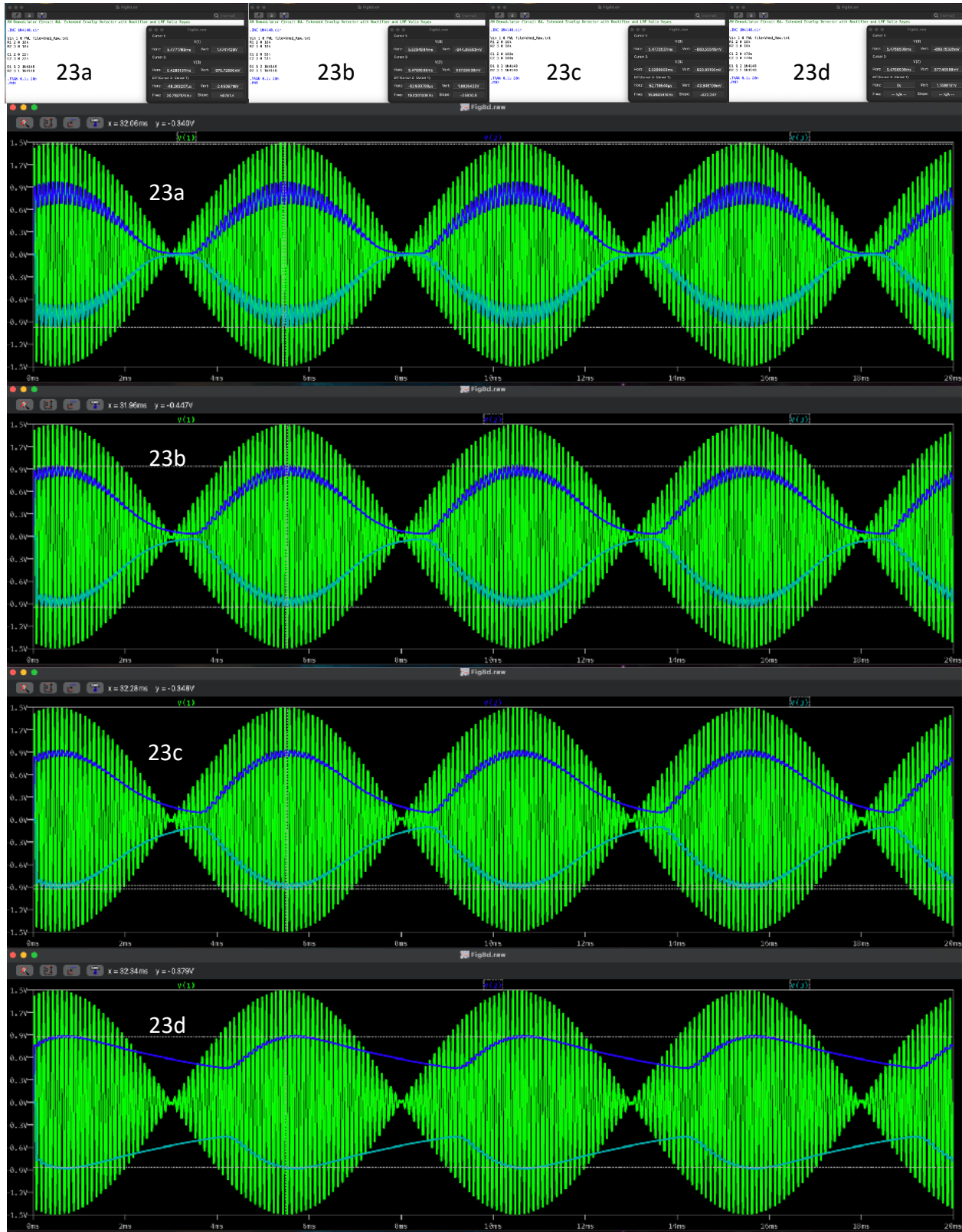


Fig. 22 Circuit from Fig 8c AM Demodulator: Extended Envelope Detector Rectifier. Image © 2024 Yolanda Reyes.

In Fig. 23, several LtSPICE plots of  $V_{in}$  vs.  $V_{out}$  were created for four scenarios: 23a.  $C_1 = 22$  [nF], 23b.  $C_1 = 53$  [nF], 23c.  $C_1 = 100$  [nF], 23d.  $C_1 = 470$  [nF]. Analysis of the LPF effects on the signal presents several options for stable system consideration, 23a - 23c, depending on the application. In the plot for simulation 23d, the signal is noticeably unacceptable and will probably result in data loss and instability within the system.

The LtSPICE simulation presented in Fig. 23 is the Extended Envelope Detector with LPF. This circuit was also presented in Fig. 8d of this report. This circuit combines a fully rectified signal  $y_{rx}(t)$ , with a LPF, which prepares  $y_{out}(t)$  ready for the next stage in the communication system, the decoder. By passing the whole signal,  $y_{rx}(t)$ , through LPF filters, we want to leverage the charge and discharge characteristics of the capacitors  $C_1$  and  $C_2$ . The goal is for  $C_1$  and  $C_2$  to respond to changes in  $V_{in}$  adequately. In a communication system, the slow roll off frequency, due to larger capacitance, may directly affect the distortion in  $y_{out}(t)$ . Some potential effects this distortion may cause would be sending the wrong combination of binary 0s and 1s and there for garbage data. Based on the LtSPICE simulations, we expect to

observe the poorest modulation index from the circuit that implements the Extended Envelope Detector with LPF using 470 [nF] and, depending on the application, perhaps the 100 [nF] iteration of the design.



**Fig. 23** Circuit from Fig 8d AM Demodulator: Extended Envelope Detector Rectifier with LPF. Image © 2024 Yolanda Reyes.

## 4. Experimental Results

Using the Scopy platform's signal generator for  $y_{det}(t)$  and oscilloscope probes on  $y_{rx}(t)$  and  $y_{out}(t)$  signals, we can confirm our theoretical and simulation work for Lab 2: AM Demodulator circuit. The first step in implementing the AM receiver demodulator circuit was to build a circuit similar to how it was presented in this report. We start with a half-wave rectifier to detect either the positive or negative half cycle of the signal  $y_{det}(t)$ . By adding an LPF, we refine our signal to have features primarily associated with the message signal  $m(t)$  portion of the  $y_{det}(t)$  and  $y_{rx}(t)$  signals.

### 4.1. Envelope Detector: Rectifier Only

The half-wave rectifier is the basic building block, and the design is implemented in forward bias, producing an output when  $y_{det}(t)$  is in the positive half-cycle of its oscillations. At this experiment stage, LtSPICE simulations are confirmed correct (see Fig. 20) and determined to predict what is observed in the lab accurately. There are peaks in Fig. 25, which will be further discussed in Section 5, Results and Conclusions, portion of this report. These peaks are observed at 1.595 [kHz], 3.187 [kHz], 3.639 [kHz], and 4.775 [kHz]. The next step is to add the low pass filter component  $C_1$ , which manages the envelope detecting and high frequency filtering LPF abilities, to the positive half-cycle of the  $y_{det}(t)$  and  $y_{rx}(t)$  signal.

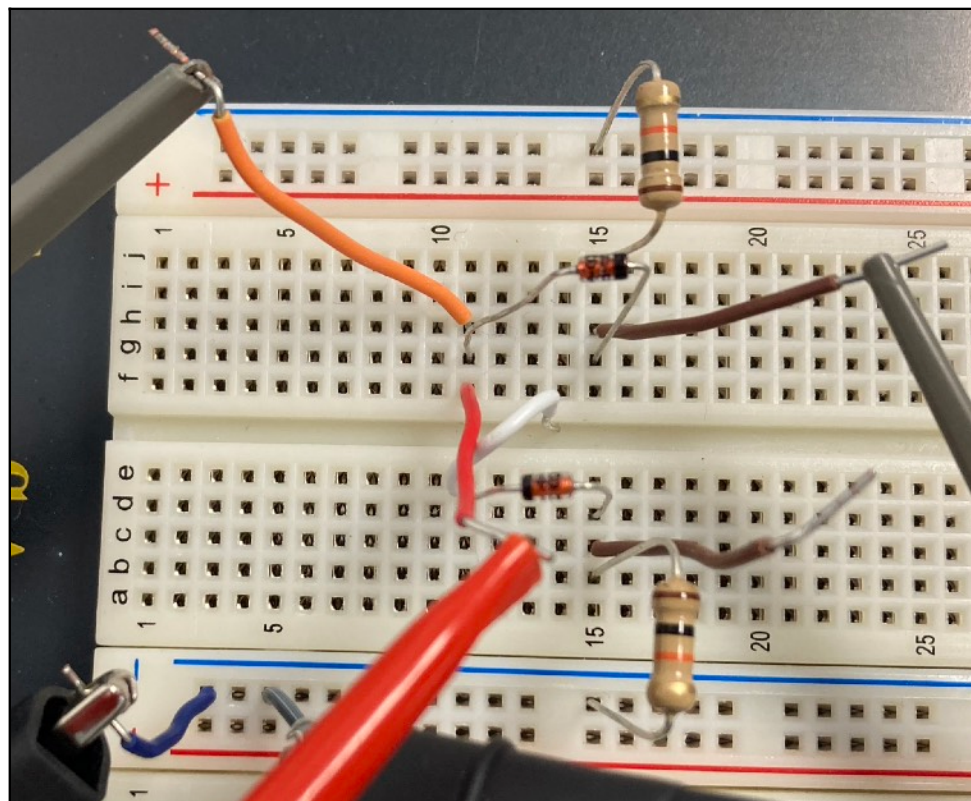
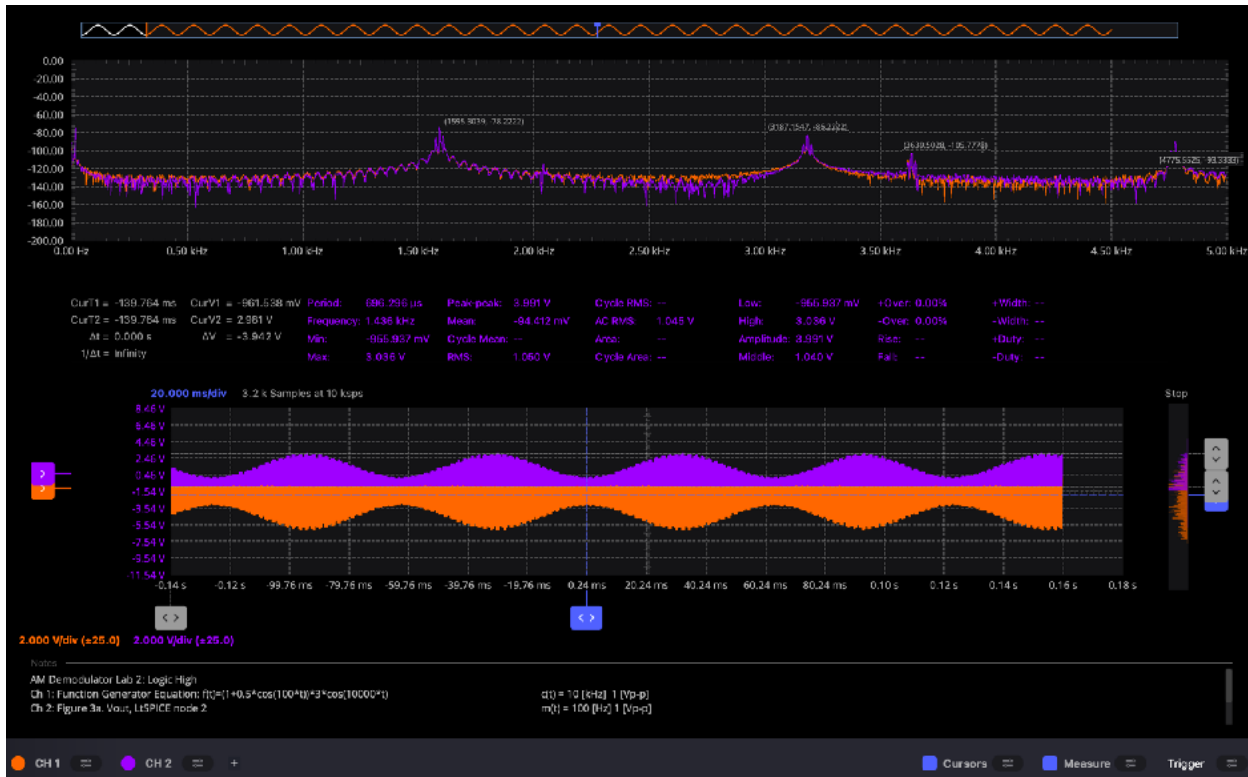
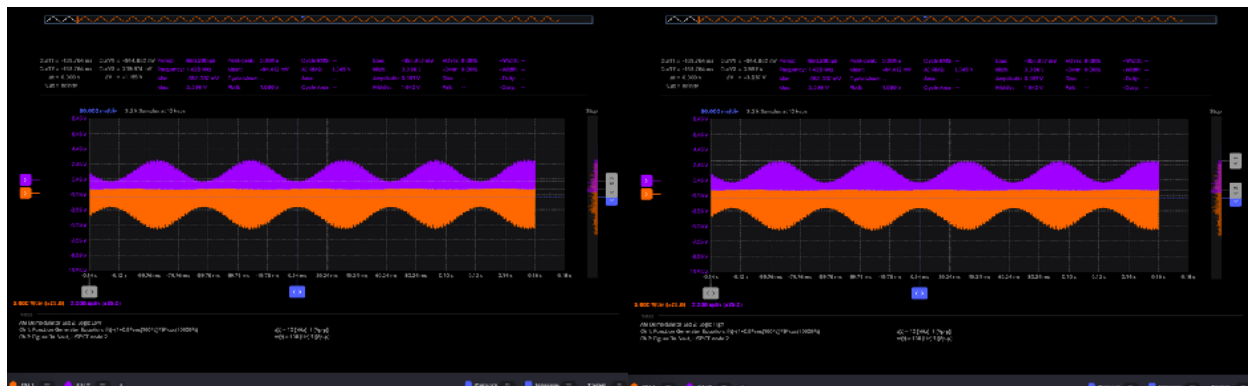


Fig. 24 Envelope Detector: Rectifier Circuit as it was implemented in the lab and presented in Fig. 8a, showcased theoretical calculations on in Fig. 13, and ran LtSPICE simulation on in Fig. 20.  
Image © 2024 Yolanda Reyes.



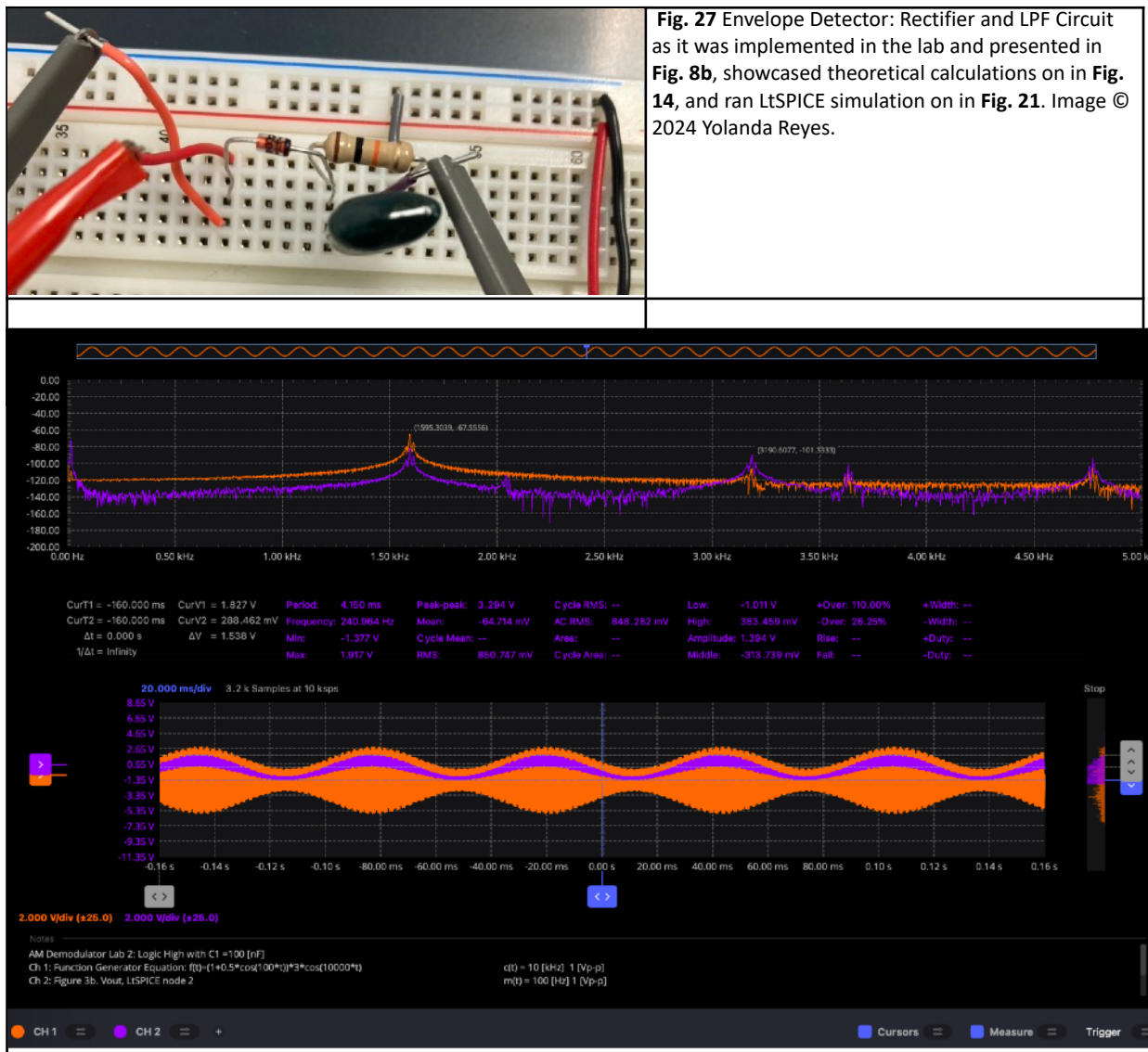
**Fig. 25** Envelope Detector: Rectifier Circuit Scopy oscilloscope and frequency plot showcasing on channel 1, in orange, the input function  $y_{det} = ((1+0.5\cos(100*t)) * 3 * \cos(10000*t)$  and on channel 2, the positive half-cycle in purple. It is important to note the frequencies associated with this circuit include 1.595 [kHz], 3.187 [kHz], 3.639 [kHz], and 4.775 [kHz]. Image © 2024 Yolanda Reyes.



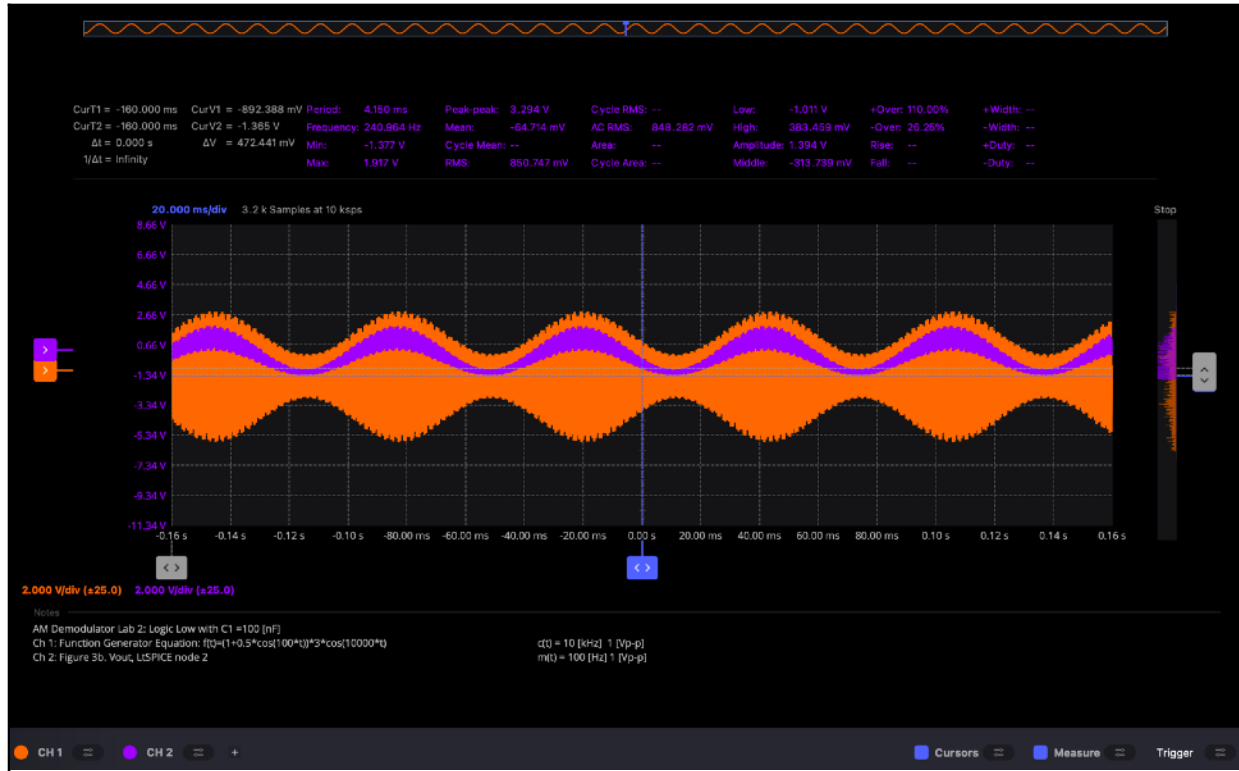
**Fig. 26** Envelope Detector: Rectifier Circuit Scopy plot showcasing on channel 1, in orange, the input function  $y_{det} = ((1+0.5\cos(100*t)) * 3 * \cos(10000*t)$  and on channel 2, the positive half-cycle in purple. It is important to note the expected voltage for binary high 1s and binary low 0s. On the left we determine logic low can include voltages up to 1.2 [v]. Logic high can be in a range no less than 1.2 [v] up to 3.937 [v]. Image © 2024 Yolanda Reyes.

## 4.2. Envelope Detector: Rectifier and LPF

With the half-wave rectifier complete, the next phase of the design process is to filter out the high frequencies associated with the carrier signal  $c(t)$  portion of the  $y_{\text{det}}(t)$  and  $y_{\text{rx}}(t)$  signal. It is essential that during filter design, the time constant  $\tau_1$  allows for adequate response from the capacitor, keeping in mind that large capacitance values for  $C_1 = 100 \text{ [nF]}$  will reduce response sensitivity. Experimental values confirm previous simulation results presented in Fig. 21. In Fig. 28 - 30, signal  $y_{\text{out}}(t)$  is presented with several features to note, such as the spikes at roughly 1.595 [kHz], 3.187 [kHz], 3.639 [kHz], and 4.775 [kHz], binary low should be no greater than  $\sim 0.945 \text{ [v]}$  and binary high in a range of voltages such that it is  $> 0.945 \text{ [v]}$  and no greater than 3.15 [v].



**Fig. 28** Envelope Detector: Rectifier and LPF Circuit Scopy oscilloscope and frequency plot showcasing on channel 1, in orange, the input function  $y_{\text{det}} = ((1 + 0.5 * \cos(100*t)) * 3 * \cos(10000*t))$  and on channel 2, the positive half-cycle in purple. It is important to note the frequencies associated with this circuit include 1.595 [kHz], 3.190 [kHz], 3.639 [kHz], and 4.775 [kHz] with  $C_1 = 100 \text{ [nF]}$ . Image © 2024 Yolanda Reyes.



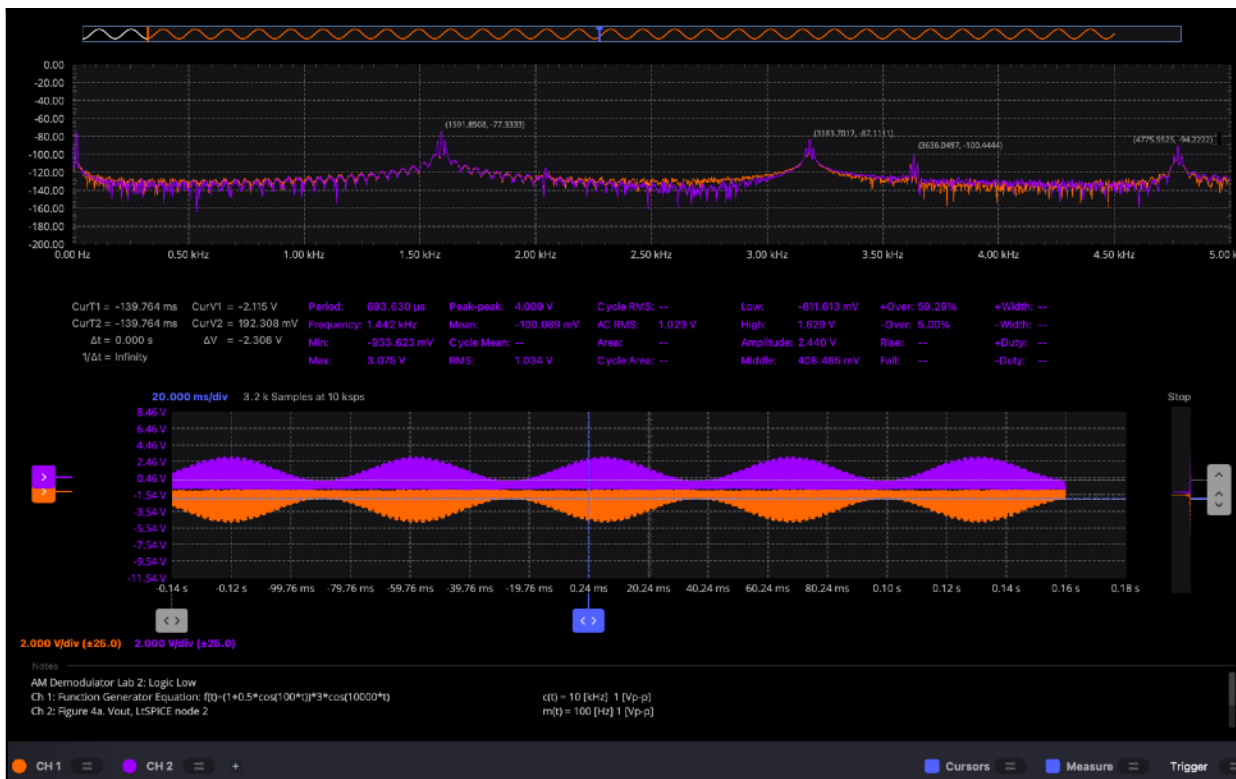
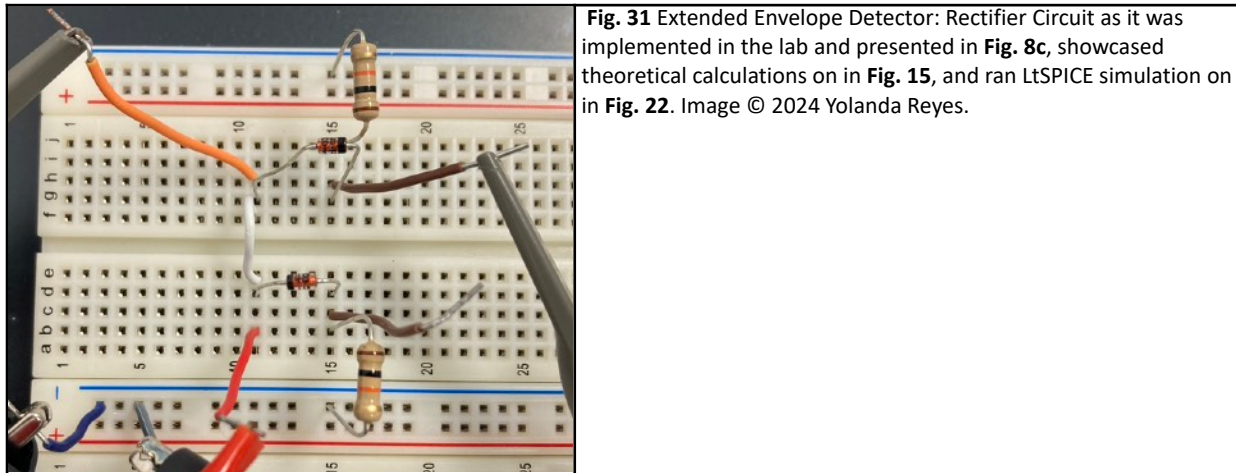
**Fig. 29 Envelope Detector: Rectifier Circuit Scopy oscilloscope and frequency plot showcasing on channel 1, in orange, the input function  $y_{\text{det}}=((1+0.5*\cos(100*t))*3 * \cos(10000*t)$  and on channel 2, the positive half-cycle in purple. It is important to note that according to the oscilloscope cursors our binary low 0s should be no greater than ~0.945 [v]. Image © 2024 Yolanda Reyes.**



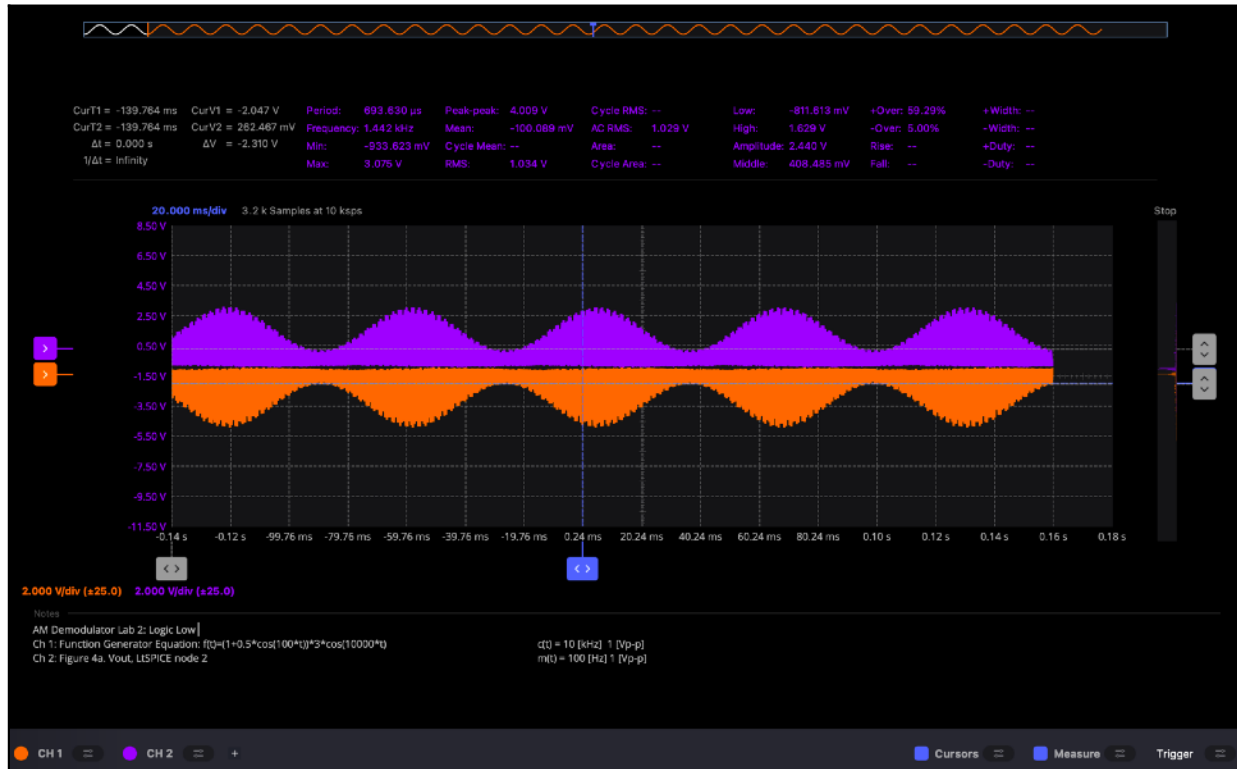
**Fig. 30 Envelope Detector: Rectifier Circuit Scopy oscilloscope and frequency plot showcasing on channel 1, in orange, the input function  $y_{\text{det}}=((1+0.5*\cos(100*t))*3 * \cos(10000*t)$  and on channel 2, the positive half-cycle in purple. It is important to note that according to the oscilloscope cursors our binary high 1s should be in a range of voltages such that it is > 0.945 [v] and no greater than 3.15 [v]. Image © 2024 Yolanda Reyes.**

### 4.3. Extended Envelope Detector: Rectifier

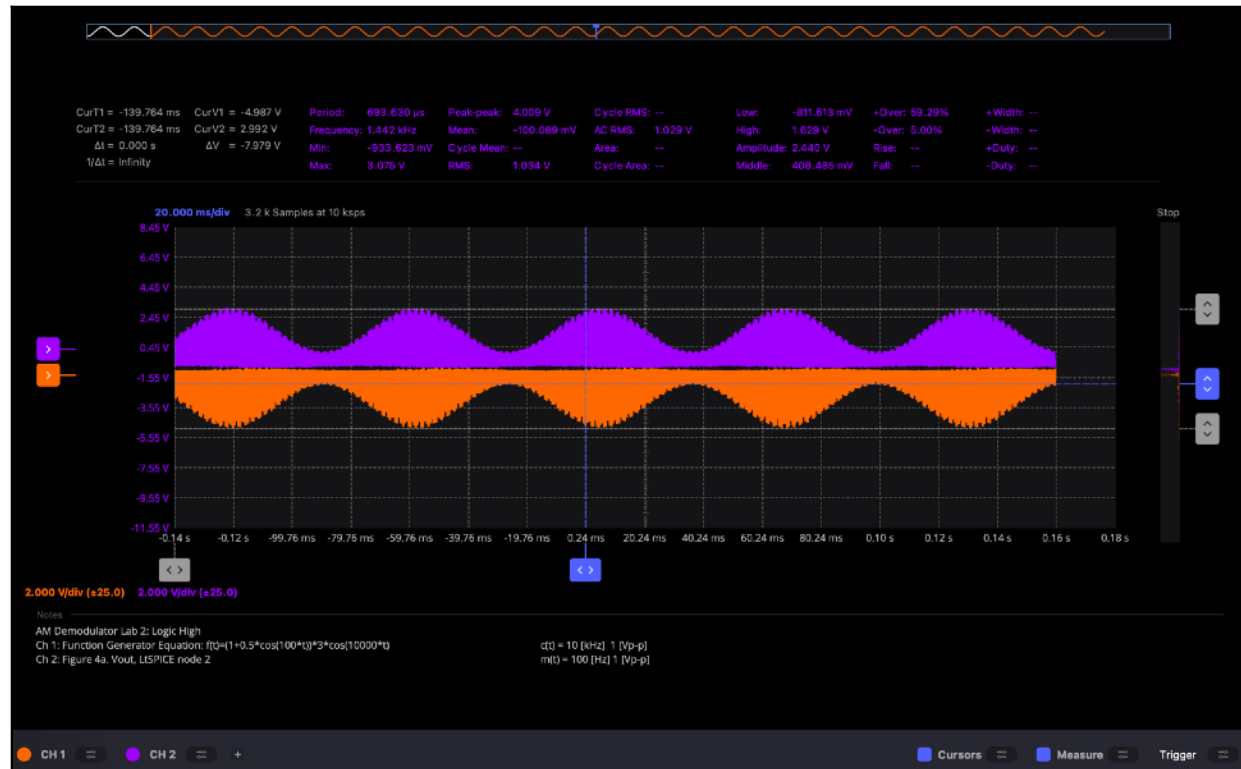
The full-wave rectifier is fully designed when implemented with components that utilize the forward bias and reverse bias diode circuit. The circuit presented in Fig. 31 produces a full output wave  $y_{out}(t)$  during all  $y_{rx}(t)$  oscillations. In Fig. 32, the same spikes at roughly 1.595 [kHz], 3.187 [kHz], 3.639 [kHz], and 4.775 [kHz] are present in the circuit as well. The range for logic low 0s is presented in Fig. 33, whereas the measurements for the range of voltages for logic high 1s are presented in Fig. 34.



**Fig. 32** Extended Envelope Detector: Rectifier Circuit Scopy oscilloscope and frequency plot showcasing on channel 1, in orange, the negative half-cycle of  $y_{rx}(t)$  and on channel 2, the positive half-cycle of  $y_{rx}(t)$  in purple. It is important to note that frequencies associated with this circuit again include 1.595 [kHz], 3.190 [kHz], 3.639 [kHz], and 4.775 [kHz] with  $C_1 = 100$  [nF]. According to the oscilloscope cursors our binary high 1s  $2.3 \leq [V_{p-p}] \leq 7.979$ . Image © 2024 Yolanda Reyes.



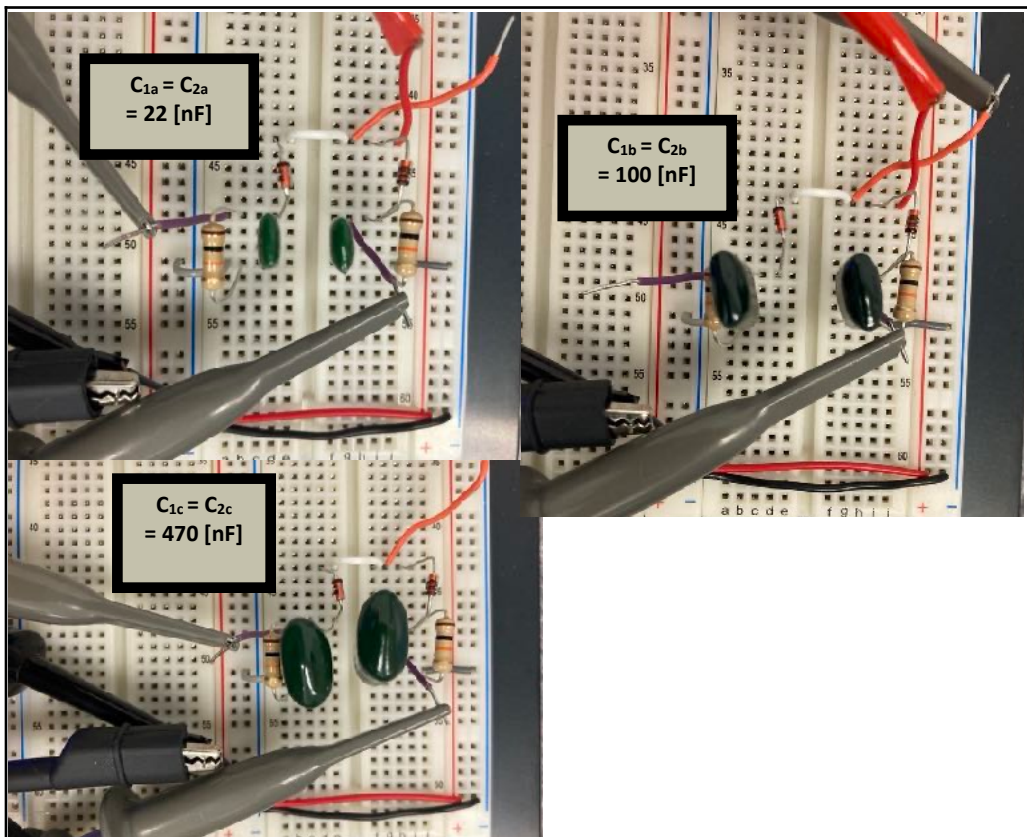
**Fig. 33** Extended Envelope Detector: Rectifier Circuit Scopy oscilloscope and frequency plot showcasing on channel 1, in orange, the negative half-cycle of  $y_{rx}(t)$  and on channel 2, the positive half-cycle of  $y_{rx}(t)$  in purple. It is important to note that according to the oscilloscope cursors our binary low 0s should be in a range of voltages such that it is  $\leq 2.3$  [V<sub>p-p</sub>]. Image © 2024 Yolanda Reyes.



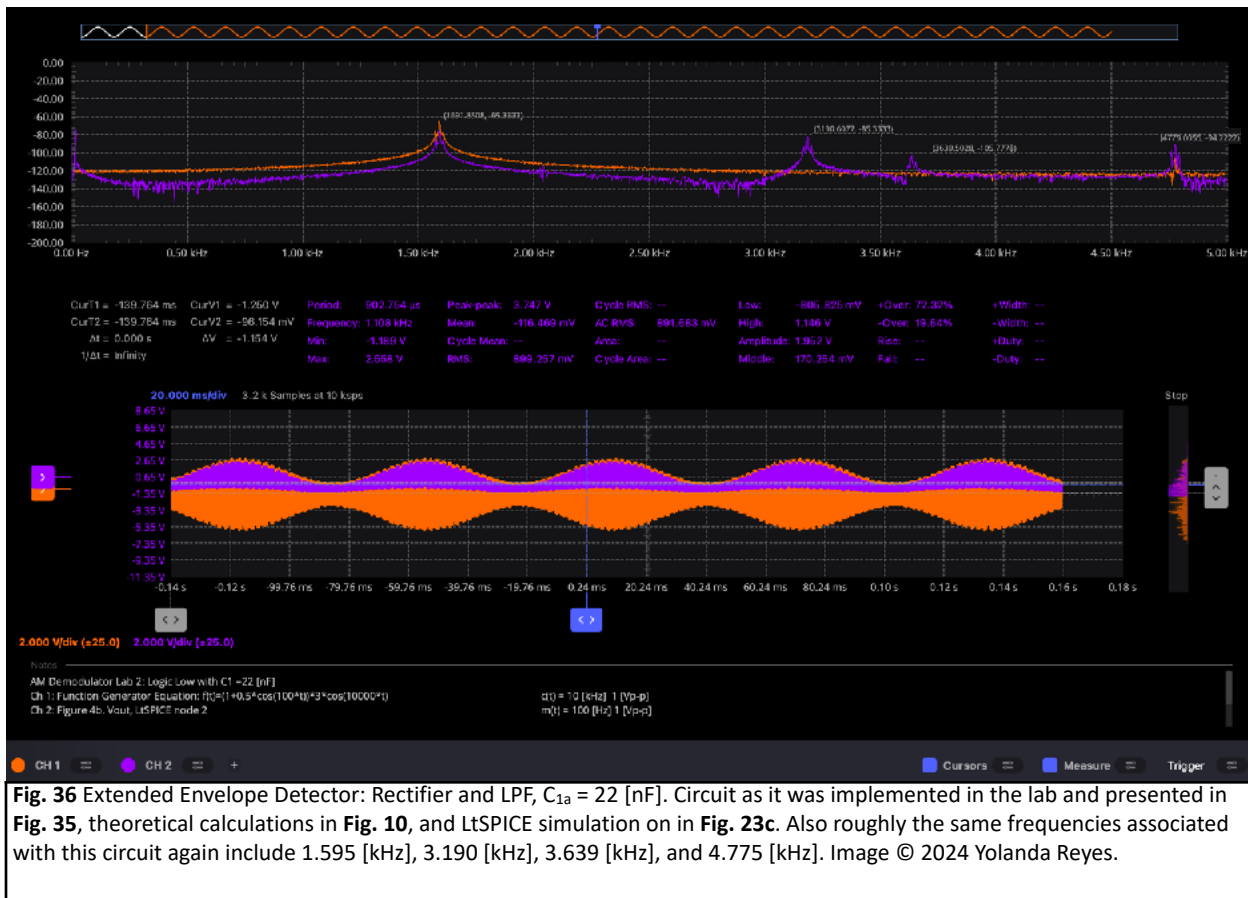
**Fig. 34** Extended Envelope Detector: Rectifier Circuit Scopy oscilloscope and frequency plot showcasing on channel 1, in orange, the negative half-cycle of  $y_{rx}(t)$  and on channel 2, the positive half-cycle of  $y_{rx}(t)$  in purple. It is important to note that according to the oscilloscope cursors our binary high 1s should be in a range of voltages such that it is  $\leq 7.979$  [V<sub>p-p</sub>]. Image © 2024 Yolanda Reyes.

#### 4.4. Extended Envelope Detector: Rectifier and LPF

With the full-wave rectifier complete, the next phase of the design process is to filter out the high frequencies associated with the carrier signal  $c(t)$  portion of the  $y_{det}(t)$  and  $y_{rx}(t)$  signal during all oscillations in positive and negative cycles. It is essential that during filter design, the time constants  $\tau_1$  and  $\tau_2$  allow for adequate response from the capacitor. Simulation results presented in Fig. 21 showcase the effects of different time constant values for  $\tau_1$ . A prominent feature to note in Fig. 36 - Fig. 40 are the type of frequencies present in  $y_{out}(t)$  as the capacitance of the components  $C_1$  and  $C_2$  varies.



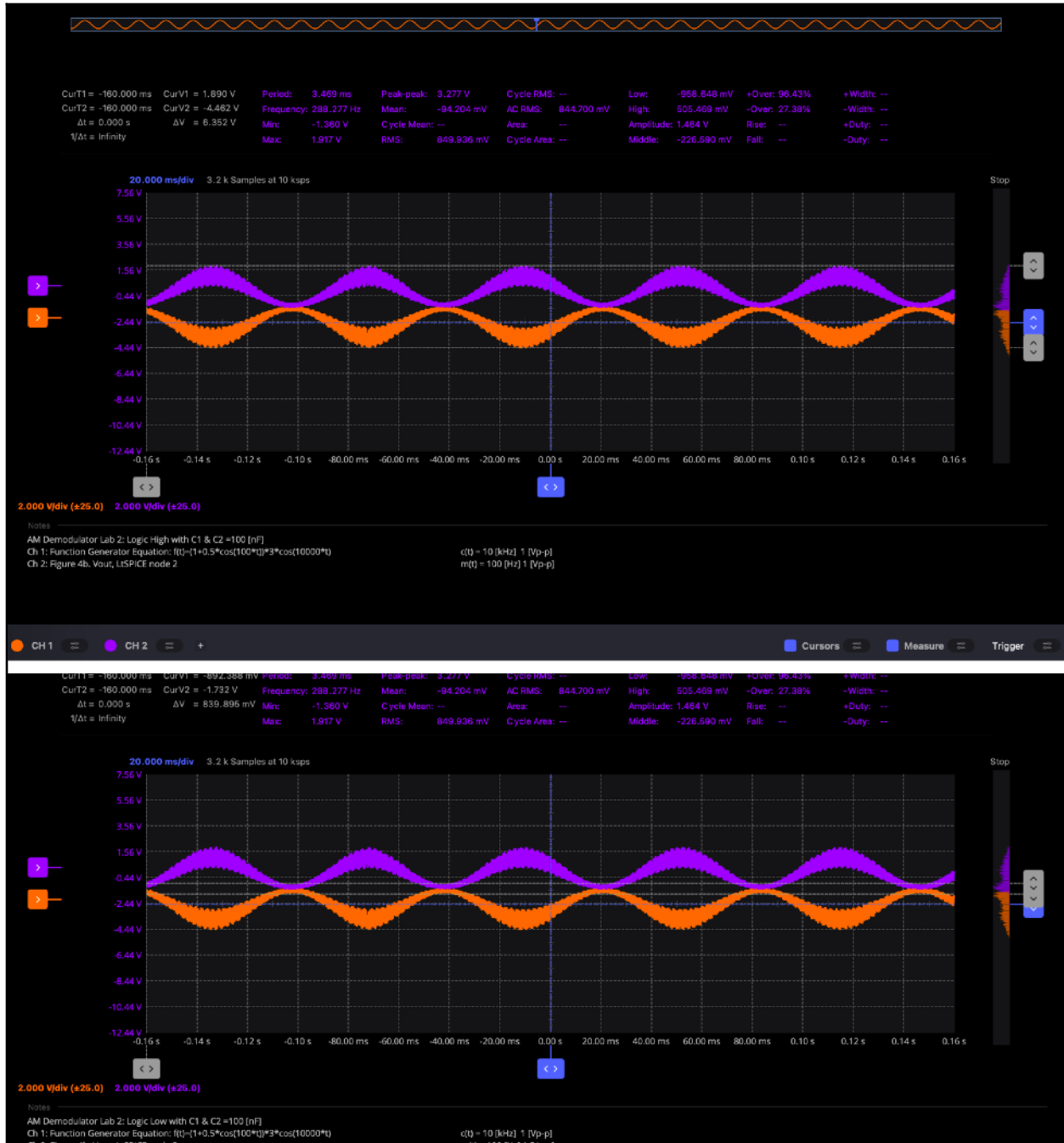
**Fig. 35** Extended Envelope Detector: Rectifier and LPF Circuit as it was implemented in the lab and presented in **Fig. 8d**, theoretical calculations showcased in **Fig. 16**, and LtSPICE simulation in **Fig. 23**. Initial value to filter above 300 [Hz] was calculated and simulated requiring a  $C_1 = 53 \text{ [nF]}$ . Due to the lack of availability of a capacitor with this value the closest above and below were chosen  $C_{1a} = 22 \text{ [nF]}$ ,  $C_{1b} = 100 \text{ [nF]}$ , and  $C_{1c} = 470 \text{ [nF]}$ . Image © 2024 Yolanda Reyes.



**Fig. 36** Extended Envelope Detector: Rectifier and LPF,  $C_{1a} = 22 \text{ [nF]}$ . Circuit as it was implemented in the lab and presented in **Fig. 35**, theoretical calculations in **Fig. 10**, and LTSpICE simulation on in **Fig. 23c**. Also roughly the same frequencies associated with this circuit again include 1.595 [kHz], 3.190 [kHz], 3.639 [kHz], and 4.775 [kHz]. Image © 2024 Yolanda Reyes.

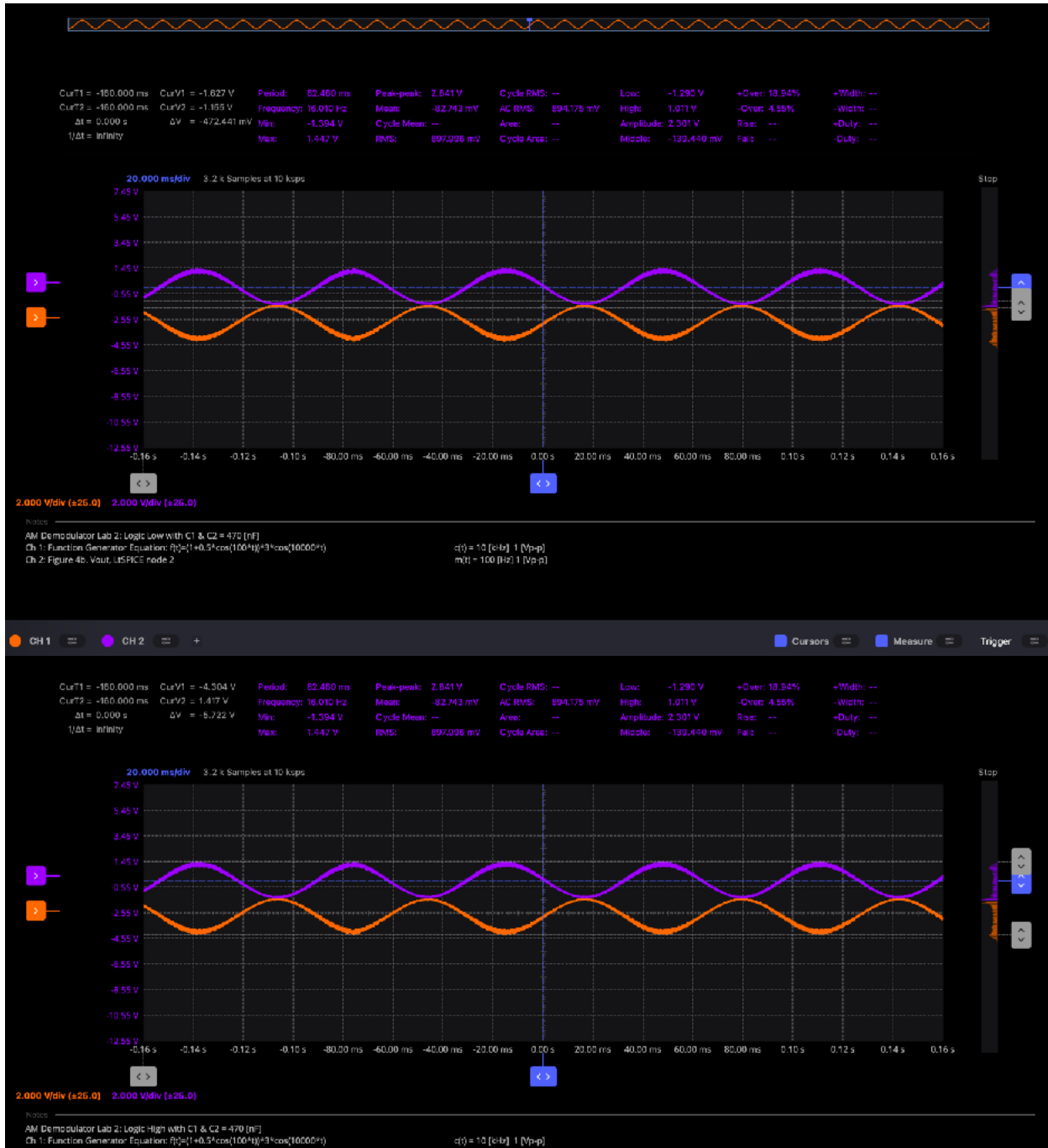


**Fig. 37** Extended Envelope Detector: Rectifier and LPF,  $C_{1a} = 22 \text{ nF}$ . Circuit as it was implemented in the lab and presented in **Fig. 35**, theoretical calculations in **Fig. 10**, and LtSPICE simulation on in **Fig. 23c**. From these experimental measurements we determine that the voltage range for binary low 0s is  $0 \text{ [V]} < y_{\text{out}}(t) \leq 1.154 \text{ [V]}$ , while the voltage range for binary high 1s is  $1.154 \text{ [V]} < y_{\text{out}}(t) \leq 2.257 \text{ [V]}$ . Image © 2024 Yolanda Reyes.



**Fig. 38** Extended Envelope Detector: Rectifier and LPF,  $C_{1b} = 100$  [nF]. Circuit as it was implemented in the lab and presented in **Fig. 35**, theoretical calculations in **Fig. 10**, and LtSPICE simulation on in **Fig. 23c**. From these experimental measurements we determine that the voltage range for binary low 0s is  $0$  [V]  $<$   $y_{out}(t) \leq 839.895$  [mV], while the voltage range for binary high 1s is  $839.895$  [mV]  $<$   $y_{out}(t) \leq 6.352$  [V]. Image © 2024 Yolanda Reyes.





**Fig. 40** Extended Envelope Detector: Rectifier and LPF,  $C_{1c} = 470 \text{ [nF]}$ . Circuit as it was implemented in the lab and presented in **Fig. 35**, theoretical calculations in **Fig. 10**, and LtSPICE simulation on in **Fig. 23c**. The voltage range for binary low 0s is  $0 \text{ [V]} < y_{\text{out}}(t) \leq 472.441 \text{ [mV]}$ , while the range for binary high 1s is  $0 \text{ } 472.441 \text{ [mV]} < y_{\text{out}}(t) \leq 5.722 \text{ [V]}$ . Image © 2024 Yolanda Reyes.

## 5. Results and Conclusion

### 5.1. Results

For Lab 2 AM Demodulator circuits were designed with varying filtering capabilities as showcased in Table 1.

Table 1

| $C_1 = C_2$<br>[nF] | Cut-Off<br>Frequency | Binary 0s<br>Logic Low  | Binary 1s<br>Logic High   | Modulation<br>Index |
|---------------------|----------------------|---|---|---------------------|
| 22                  | 723.432              | $0 \text{ [V]} < y_{\text{out}}(t) \leq 1.154 \text{ [V]}$    | $1.154 \text{ [V]} < y_{\text{out}}(t) \leq 2.257 \text{ [V]}$    | 51.13%              |
| 100                 | 159.155              | $0 \text{ [V]} < y_{\text{out}}(t) \leq 839.895 \text{ [mV]}$ | $839.895 \text{ [mV]} < y_{\text{out}}(t) \leq 6.352 \text{ [V]}$ | 13.22%              |
| 470                 | 33.86                | $0 \text{ [V]} < y_{\text{out}}(t) \leq 472.441 \text{ [mV]}$ | $472.441 \text{ [mV]} < y_{\text{out}}(t) \leq 5.722 \text{ [V]}$ | 8.26%               |

### 5.2. Discussion

The calculations finding the time domain to frequency domain transformations proved unnecessarily challenging to manage. Initially, a primary question concerning how the transform to the frequency domain should have been executed led to some questionable value of  $\pm 9700 \text{ [Hz]}$  being calculated as a potential spike for consideration. Some questions remain about a side lobe calculated at  $\pm 9700 \text{ [Hz]}$  and if there is ever an odd number of side lobes. Future research into the side lobes of the signal would be beneficial in expanding the understanding of the calculated  $\pm 9700 \text{ [Hz]}$  term. The leading theory is that it was simple mathematical error. While Lab 2 explored an AM RF communication system more in-depth, additional areas of interest include understanding how  $y_{\text{out}}(t)$  is coded/decoded and how the message signal  $m(t)$  is implemented to modulate the carrier signal  $c(t)$ . The lab work performed so far has presented several questions, such as how is  $y_{\text{det}}(t)$  switched rapidly to communicate over a channel efficiently. Future work to compare the AM and QAM modulation schemes to determine the best scheme for a particular application may be a final topic to present.

After conducting the experiments with an AM Demodulator circuit, it is not surprising that if the modulation index will change if the capacitance increases. As the capacitance increases in the circuit, the voltage will drop slowly before the capacitor can charge again. With a larger capacitance, the response of the envelope detector is not tuned, and it becomes harder to determine a binary 0 or 1. Initially, it was arbitrarily chosen to try to limit frequencies above 300 [Hz]. Further research into the workflow to determine the cut-off frequency would greatly help to fully understand the RF communication system

design process. It is important to note as well that due to the lack of availability of 53 [nF] capacitors, 22 [nF] and 100 [nF] were selected instead. While the experiment results are the correct values I should have observed I am unable to explain the frequency plot values of 1.595 [kHz], 3.190 [kHz], 3.639 [kHz], and 4.775 [kHz] which are presented in Fig.32, Fig. 36, and Fig. 39.

### **5.3. Conclusion**

Analyzing an AM Demodulating circuit and observing the characteristics associated with filtering different cut-off frequencies requires the application of many topics covered in electrical and computer engineering. A good understanding of how to apply transforms such as Z-Domain and Frequency Domain enables a designer to determine how stable the filter is and confirm the region of operation. For Lab 2, the region of operation was determined to be a low pass filter (LPF). An LPF was used because, in the communication system design, the message signal  $m(t)$  representing the data to be communicated occupies lower frequencies than the carrier signal  $c(t)$ . Metrics not fully covered in this report include the signal-to-noise ratio and Bit Error Rate. Results presented in Table 1. give insight into the Bit Error Rate since the modulation index quantifies how likely a system can differentiate between a binary 0 and binary 1. One design choice that significantly affects a system's ability to recover the correct information is if the time constant of the RC circuit in the demodulator is tuned appropriately. The goal with the time constant is to pick components that provide a satisfactory signal response such that there is no attenuation of the signal to be decoded.

## 6. Diode: 1N4148 Datasheet

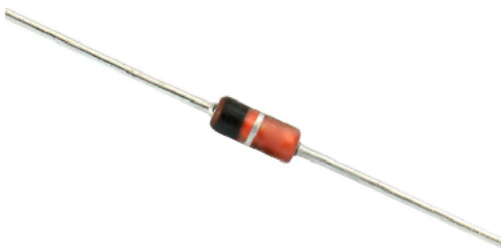


[www.vishay.com](http://www.vishay.com)

**1N4148**

Vishay Semiconductors

### Small Signal Fast Switching Diodes



#### FEATURES

- Silicon epitaxial planar diode
- Electrically equivalent diodes: 1N4148 - 1N914
- Material categorization:  
For definitions of compliance please see [www.vishay.com/doc?99912](http://www.vishay.com/doc?99912)



**RoHS**  
COMPLIANT  
HALOGEN  
**FREE**

#### APPLICATIONS

- Extreme fast switches

#### MECHANICAL DATA

**Case:** DO-35

**Weight:** approx. 105 mg

**Cathode band color:** black

**Packaging codes/options:**

TR/10K per 13" reel (52 mm tape), 50K/box

TAP/10K per ammopack (52 mm tape), 50K/box

#### PARTS TABLE

| PART   | ORDERING CODE          | TYPE MARKING | INTERNAL CONSTRUCTION | REMARKS                |
|--------|------------------------|--------------|-----------------------|------------------------|
| 1N4148 | 1N4148-TAP or 1N4148TR | V4148        | Single diode          | Tape and reel/ammopack |

#### ABSOLUTE MAXIMUM RATINGS ( $T_{amb} = 25^{\circ}\text{C}$ , unless otherwise specified)

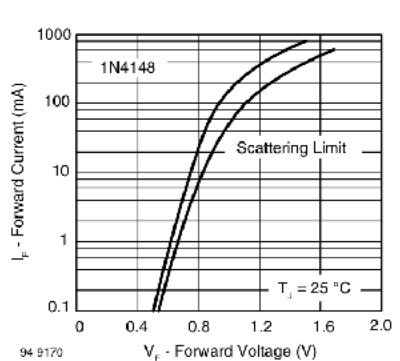
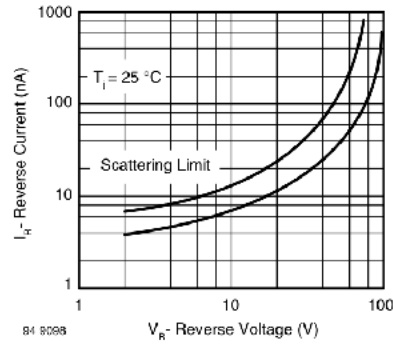
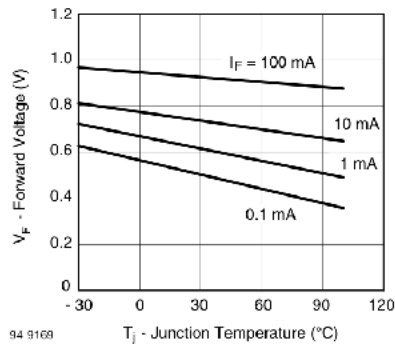
| PARAMETER                       | TEST CONDITION                                  | SYMBOL      | VALUE | UNIT |
|---------------------------------|---|-------------|-------|------|
| Repetitive peak reverse voltage |   | $V_{RRM}$   | 100   | V    |
| Reverse voltage                 |   | $V_R$       | 75    | V    |
| Peak forward surge current      | $t_o = 1 \mu\text{s}$                           | $I_{FSM}$   | 2     | A    |
| Repetitive peak forward current |   | $I_{FRM}$   | 500   | mA   |
| Forward continuous current      |   | $I_F$       | 300   | mA   |
| Average forward current         | $V_R = 0$                                       | $I_{F(AV)}$ | 150   | mA   |
| Power dissipation               | $I = 4 \text{ mm}, T_L = 45^{\circ}\text{C}$    | $P_{tot}$   | 440   | mW   |
|                                 | $I = 4 \text{ mm}, T_L \leq 25^{\circ}\text{C}$ | $P_{tot}$   | 500   | mW   |

#### THERMAL CHARACTERISTICS ( $T_{amb} = 25^{\circ}\text{C}$ , unless otherwise specified)

| PARAMETER                                  | TEST CONDITION                            | SYMBOL     | VALUE       | UNIT |
|--|---|------------|-------------|------|
| Thermal resistance junction to ambient air | $I = 4 \text{ mm}, T_L = \text{constant}$ | $R_{ThJA}$ | 350         | K/W  |
| Junction temperature                       |   | $T_j$      | 175         | °C   |
| Storage temperature range                  |   | $T_{stg}$  | -65 to +150 | °C   |

**ELECTRICAL CHARACTERISTICS** ( $T_{amb} = 25^{\circ}\text{C}$ , unless otherwise specified)

| PARAMETER                | TEST CONDITION   | SYMBOL     | MIN. | TYP. | MAX. | UNIT |
|--------------------------|--|------------|------|------|------|------|
| Forward voltage          | $I_F = 10 \text{ mA}$  | $V_F$      |      |      | 1    | V    |
|                          | $V_R = 20 \text{ V}$   | $I_R$      |      |      | 25   | nA   |
| Reverse current          | $V_R = 20 \text{ V}, T_j = 150^{\circ}\text{C}$                                  | $I_R$      |      |      | 50   | μA   |
|                          | $V_R = 75 \text{ V}$   | $I_R$      |      |      | 5    | μA   |
| Breakdown voltage        | $I_R = 100 \mu\text{A}, t_p/T = 0.01, t_p = 0.3 \text{ ms}$                      | $V_{(BR)}$ | 100  |      |      | V    |
| Diode capacitance        | $V_R = 0 \text{ V}, f = 1 \text{ MHz}, V_{HF} = 50 \text{ mV}$                   | $C_D$      |      |      | 4    | pF   |
| Rectification efficiency | $V_{HF} = 2 \text{ V}, f = 100 \text{ MHz}$                                      | $\eta_r$   | 45   |      |      | %    |
| Reverse recovery time    | $I_F = I_R = 10 \text{ mA}, i_R = 1 \text{ mA}$                                  | $t_{rr}$   |      |      | 8    | ns   |
|                          | $I_F = 10 \text{ mA}, V_R = 6 \text{ V}, i_R = 0.1 \times I_R, R_L = 100 \Omega$ | $t_{rr}$   |      |      | 4    | ns   |

**TYPICAL CHARACTERISTICS** ( $T_{amb} = 25^{\circ}\text{C}$ , unless otherwise specified)


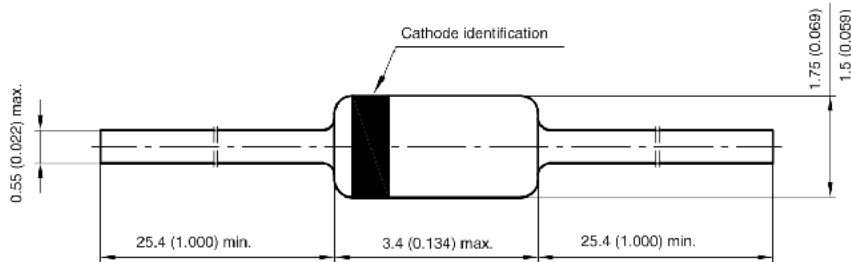


[www.vishay.com](http://www.vishay.com)

**1N4148**

Vishay Semiconductors

**PACKAGE DIMENSIONS** in millimeters (inches): **DO-35\_02**



Document no.: 6.560-5004.12-4  
Created - Date: 17. March 2008  
21148

## 7. References

- [1] Heilbron, J. L. (ed.), "The Oxford Guide to the History of Physics and Astronomy", Oxford, UK: Oxford University Press, 2005, pp. 148.
- [2] T. White, "United States Early Radio History," *Word Origins-Radio*, section 22. Accessed: Sept. 18, 2024. [Online]. Available: <https://earlyradiohistory.us/sec022.htm.\>
- [3] Belrose, J., "Marconi and the History of Radio," *IEEE Antennas and Propagation Magazine*, Vol. 46, No. 2, 2004, pp.130
- [4] International Telecommunications Union, G.711: Pulse Code Modulation (PCM) of Voice Frequencies. Accessed: Sept. 18, 2024. [Online]. Available: <http://www.itu.int/rec/T-REC-G.711/>
- [5] Hauben, R., "From the ARPANET to the Internet," *TCP Digest(UUCP)*, January 2001. Accessed: Sept. 18, 2024. [Online]. Available: [http://www.columbia.edu/~rh120/other/tcpdigest\\_paper.txt](http://www.columbia.edu/~rh120/other/tcpdigest_paper.txt)
- [6] International Telecommunications Union, G.722: 7 kHz Audio-Coding within 64 kbit/s, Accessed: Sept. 18, 2024. [Online]. Available: <https://www.itu.int/rec/T-REC-G.722>
- [7] Kilby, J., *Miniatrized Electronic Circuits*, 1964, US Patent No. 3,138,743. Accessed: Sept. 18, 2024. [Online]. Available: <https://www.google.com/patents/US3138743>
- [8] Moore, G., Lithography and the Future of Moore's Law," *SPIE*, Vol.2438, 1995. Accessed: Sept. 18, 2024. [Online]. Available: <http://www.lithoguru.com/scientist/CHE323/Moore1995.pdf>
- [9] Kester, W., *The Data Conversion Handbook*, Analog Devices, 2005. Accessed: Sept. 18, 2024. [Online]. Available: <http://www.analog.com/en/education/education-library/data-conversion-handbook.html>
- [10] Hall, B., and W. Taylor, "X- and Ju-Band Samll Form Factor Radio Design," Analog Devices Inc., Wilmington, MA, 2017. Accessed: Sept. 18, 2024. [Online]. Available: <http://www.analog.com/en/technical-articles/x-and-ku-band-small-form-factor-radio-design.html>
- [11] Pickle, B. "Modulation", Sharpened Productions, Accessed: Sept. 18, 2024. [Online]. Available: <https://techterms.com/definition/modulation>

- [12] H. Kwasme and S. Ekin, "RSSI-Based Localization Using LoRaWAN Technology," IEEE Access, vol. 7, pp. 99856-99866, 2019. Accessed: Sept. 18, 2024. [Online]. Available: <https://ieeexplore.ieee.org/document/8764340>